Published OnlineFirst September 9, 2014; DOI: 10.1158/0008-5472.CAN-14-0254

Cancer Research

Metabolic Vulnerabilities in Endometrial Cancer

Frances L. Byrne[1,2], Ivan K.H. Poon[3,4], Susan C. Modesitt[5], Jose L. Tomsig[1], Jenny D.Y. Chow[1], Marin E. Healy[1], William D. Baker[5], Kristen A. Atkins[6], Johnathan M. Lancaster[7], Douglas C. Marchion[7], Kelle H. Moley[8], Kodi S. Ravichandran[3,9], Jill K. Slack-Davis[3,10], and Kyle L. Hoehn[1,2,10,11]

Abstract

Women with metabolic disorders, including obesity and diabetes, have an increased risk of developing endometrial cancer. However, the metabolism of endometrial tumors themselves has been largely understudied. Comparing human endometrial tumors and cells with their nonmalignant counterparts, we found that upregulation of the glucose transporter GLUT6 was more closely associated with the cancer phenotype than other hallmark cancer genes, including hexokinase 2 and pyruvate kinase M2. Importantly, suppression of GLUT6 expression inhibited glycolysis and survival of endometrial cancer cells. Glycolysis and lipogenesis were also highly coupled with the cancer phenotype in patient samples and cells. To test whether targeting endometrial cancer metabolism could be exploited as a therapeutic strategy, we screened a panel of compounds known to target diverse metabolic pathways in endometrial cells. We identified that the glycolytic inhibitor, 3-bromopyruvate, is a powerful antagonist of lipogenesis through pyruvylation of CoA. We also provide evidence that 3-bromopyruvate promotes cell death via a necrotic mechanism that does not involve reactive oxygen species and that 3-bromopyruvate impaired the growth of endometrial cancer xenografts *Cancer Res; 74(20); 1–14. ©2014 AACR.*

Introduction

Endometrial cancer is the most common gynecologic malignancy in the developed world and affects more than 287,000 women and attributes to 74,000 deaths worldwide each year (1). Endometrial tumors originate from epithelial cells of the uterus and may locally progress to invade the myometrium and further metastasize to lymph nodes, liver, and lungs in advanced stages (2). Endometrial cancer most commonly arises in postmenopausal women and is classically categorized in two clinicopathologic subtypes: type I (endometrioid) and type II (predominantly clear cell and papillary serous). Type II tumors are generally more invasive, estrogen receptor and progesterone receptor (ER/PR) negative, and confer a poor prognosis but account for less than 15% of all cases (3, 4). In contrast, the more common type I tumors are frequently low-grade, noninvasive, ER/PR-positive, and survival rates are higher due to early identification and treatment with primary surgery (4).

Obesity [body mass index (BMI) > 30 kg/m^2] is associated with increased incidence, risk of death, and lower age of diagnosis for endometrial cancer (5–7). Disorders associated with hyperglycemia (type 1 and 2 diabetes) also have increased risk of endometrial cancer, indicating that poor control of blood glucose may be an important contributor to the growth of these tumors in women (8, 9). In our previous study comparing obese women with and without type I endometrial cancer, circulating glucose levels were higher in women with cancer (119.5 vs. 90.7 mg/dL for noncancer; $P = 0.049$). However, other cancer-related parameters including estrogen and insulin were not significantly elevated in obese women with cancer (10). These findings suggested that, independent of adiposity and its associated hormonal changes, increased blood glucose levels may play an important role in the growth and/or development of type I endometrial cancer.

Endometrial cancers are well-studied at the genetic level, but few studies have rigorously evaluated endometrial cancer metabolism. Many of the genetic aberrations that are thought to drive endometrial cancer initiation and progression also regulate cell metabolism. For example, the PI3K/protein kinase B (Akt) pathway is altered in up to 93% of type I endometrial tumors, through loss of PTEN and mutations in PI3K family members (4, 11). Other aberrations include mutations in V-Ki-

[1]Department of Pharmacology, University of Virginia, Charlottesville, Virginia. [2]School of Biotechnology and Biomolecular Sciences, University of New South Wales, Sydney, Australia. [3]Department of Microbiology, Immunology, and Cancer Biology, University of Virginia, Charlottesville, Virginia. [4]Department of Biochemistry, La Trobe Institute for Molecular Science, La Trobe University, Victoria, Australia. [5]Department of Obstetrics and Gynecology, University of Virginia, Charlottesville, Virginia. [6]Department of Pathology, University of Virginia, Charlottesville, Virginia. [7]Departments of Women's Oncology and Experimental Therapeutics Program, H. Lee Moffitt Cancer Center and Research Institute, Tampa, Florida. [8]Department of Obstetrics and Gynecology, Washington University School of Medicine, St. Louis, Missouri. [9]Center for Cell Clearance, University of Virginia, Charlottesville, Virginia. [10]Cancer Center, University of Virginia, Charlottesville, Virginia. [11]Department of Medicine, University of Virginia, Charlottesville, Virginia.

Note: Supplementary data for this article are available at Cancer Research Online (http://cancerres.aacrjournals.org/).

Corresponding Author: Kyle L. Hoehn, University of Virginia, 5224 Jordan Hall, PO Box 800735, Charlottesville, VA 22908. Phone: 612-9385-9399; Fax: 434-982-3878; E-mail: klh8st@virginia.edu

doi: 10.1158/0008-5472.CAN-14-0254

Published OnlineFirst September 9, 2014; DOI: 10.1158/0008-5472.CAN-14-0254

ras2 Kirsten rat sarcoma viral oncogene homolog, overexpression of epidermal growth factor receptor, loss of liver kinase B1 (LKB1), and tuberous sclerosis 2 (TSC2; refs. 4, 12, 13). Despite this information, it remains unclear whether the flux of nutrients through metabolic pathways contributes to endometrial cancer cell survival and tumor growth. Herein, we show that glycolytic–lipogenic metabolism is increased in endometrial cancer cells and that they are dependent upon this metabolism for survival.

Materials and Methods

Patient sample analyses

Institutional review board approval, in accordance with Federal regulations, was obtained from the University of Virginia Health System (Charlottesville, VA). Endometrial samples were collected at surgery (hysterectomy) from four women with and four women without type I endometrial cancer (mean age, 52.6 years; BMI, 44.5 kg/m^2) and RNA was analyzed, as described (14). For protein expression analyses, nontumor and tumor endometrial tissue (matched for each patient) were obtained from an independent cohort of postmenopausal women (mean BMI, 35.3 kg/m^2), with Federation Internationale des Gynaecologistes et Obstetristes (FIGO)-defined low-stage (1A–1C) and grade (1–2) type I endometrial cancer. Analyses of gene alterations (shown in Table 1) from endometrial and ovarian cancers were performed using cBioPortal (15, 16) and are based solely upon data generated by The Cancer Genome Atlas (TCGA) Research Network (11, 17, 18).

Endometrial cells

Cells were obtained from ATCC (HEC-1-A, AN3CA, KLE, RL95-2); Sigma Aldrich (Ishikawa); Deutsche Sammlung von Mikroorganismen und Zellkulturen (MFE-296, MFE-319); Dr. Hui Li at the University of Virginia (MAD11) and Dr. Kelle Moley at Washington University School of Medicine, St. Louis, MO (hUE-Ts). MAD11 and hUE-Ts are human telomerase reverse transcriptase (hTERT)-immortalized endometrial stromal and uterine epithelial cells, respectively, which were both derived from patients without cancer. Cancer cells have not been validated since purchase.

Immunohistochemistry

Pathologic analyses of tumor and nontumor tissue were performed by a certified gynecologic oncology pathologist in a blinded manner. Immunohistochemistry was performed at the University of Virginia Biorepository and Tissue Research Facility using a mouse monoclonal antibody against human GLUT6 (Abcam). 3,3′-Diaminobenzidine was used as a substrate for the peroxidase reaction and hematoxylin as the counterstain. Slides were scanned using an Aperio ScanScope XT Slide Scanner (Aperio) and images analyzed using the ImageScope software (Aperio).

siRNA transfections

Cells were double transfected (24 hours apart) with 50 nmol/L ON-TARGETplus siRNA; *SLC2A6* (GLUT6) SMARTpool (Pool), GLUT6 individual siRNA sequences found in the SMARTpool (Seq.1-4), or equivalent concentrations of nontargeting SMARTpool control (Ctrl) siRNA (ThermoFisher Scientific) using JetPRIME reagent (Polyplus Transfection Inc.) as the delivery vehicle.

qPCR

RNA was isolated with TRIzol reagent (Life Technologies) and reverse transcribed using a High Capacity cDNA kit (Life Technologies). qPCR was performed using iQ SYBR Green SuperMix (Bio-Rad) on an iCycler (MyiQ Optical Module)

Table 1. Glycolytic–lipogenic gene alterations in gynecologic malignancies

Cancer	Total cases	Cases with gene alterations (%)	Cases with genes only downregulated	Survival *P*
Endometrial type I	307	123 (40)	4	0.003384[a]
Stage I	231	88 (38)	4	0.241869
Stages II–IV	76	35 (46)	0	0.023995[a]
All stages lean (BMI < 30)	109	51 (47)	2	0.381992
All stages obese (BMI ≥ 30)	195	71 (36)	2	0.007452[a]
Endometrial type II	66	45 (68)	0	0.967244
Stage I	23	16 (70)	0	0.294052
Stages II–IV	43	29 (67)	0	0.611672
All stages lean (BMI < 30)	33	23 (70)	0	0.826925
All stages obese (BMI ≥ 30)	33	22 (67)	0	0.751774
Ovarian	316	254 (80)	78	0.580492

NOTE: Analyses were performed on cBioPortal using uterine corpus endometrial carcinoma (TCGA; ref. 11) and ovarian serous cystadenocarcinoma (TCGA; ref. 17) datasets. Genes included in the analysis were GLUT6, HK2, PFKP, LDHA, ENO1, GAPDH, BPGM, ENO2, ALDOA, PKM2, ACLY, ACC1, ACC2, and FASN. Alterations considered were mRNA expression (up- or downregulated), gene amplification, deletion, and mutations.

[a]Significantly worse survival ($P < 0.05$) compared with those cases (within a type of cancer) without these alterations.

Published OnlineFirst September 9, 2014; DOI: 10.1158/0008-5472.CAN-14-0254

Bio-Rad system. GLUT mRNA expression was normalized to β2M using the Pffafl method (19).

Western blotting

Protein lysates (20μg) were resolved by PAGE and electrotransferred to nitrocellulose membrane. Protein expression was detected with rabbit antibodies such as GAPDH, PKM2, LDHA, ACLY, ACC, FASN, PTEN, AKT, PPARγ, TSC2, G6PD (Cell Signaling Technology); GLUT1 (Abcam); and mouse antibodies such as pAKT (S473), P-p70S6 kinase (T389) (Cell Signaling Technology); HK2, MCT1, 14-3-3 (Santa Cruz); GLUT6 (Abcam); and β-actin (Sigma Aldrich). Primary antibodies were detected with goat anti-mouse IgG (DyLight 800 conjugate) or anti-rabbit IgG (DyLight 680 conjugate) and membranes scanned on the LI-COR ODYSSEY System (LI-COR).

Metabolic assays

Cells were incubated in Krebs Ringer Phosphate (KRP) nutrient buffer containing either D-[3-^{3}H] glucose, D-[^{14}C(U)] glucose, L[^{14}C(U)]-glutamic acid, [1-^{14}C]-palmitic acid, or [2-^{14}C] acetic acid sodium salt. Substrate oxidation was measured capturing evolved $^{14}CO_2$ and *de novo* lipogenesis (DNL) from substrates was measured by hexane:isopropanol (3:2) extraction of ^{14}C-lipids. For glycolysis measurements, D-[3-^{3}H] glucose was separated from tritiated $[^{3}H]_2O$ by diffusion. Detailed methods for these assays are provided in Supplementary Material. For OCR and ECAR measurements, cells (10,000 to 20,000/well) were seeded in 24-well Seahorse tissue culture plates a day before incubation in KRP nutrient buffer (37°C for >30 minutes). Basal OCR (pmolesO_2/min) and ECAR (mpH/min) were measured using the Seahorse XF-24 Flux Analyzer (Seahorse Biosciences). OCR and ECAR rates for each cell line were averaged over 3 plates and normalized to protein content per well.

Lactate release

Lactate standards, NAD^+, and lactate dehydrogenase (LDH) were prepared in glycine–hydrazine buffer (500 mmol/L glycine, 127 mmol/L hydrazine sulfate, pH 9.5). Cells were incubated in DMEM (without phenol red or FBS) for 45 minutes. Media removed from cells was incubated with 2.5 mmol/L NAD^+ and 25 μg/mL LDH for 1 hour at room temperature and absorbance measured at 340 nm.

Glucose uptake

Cells were incubated with 5 mmol/L 2-deoxy-D-glucose (2-DG) in KRP with 0.2 μCi of ^{3}H-2-DG per well for 2.5 minutes. Cells were rinsed twice in ice-cold PBS before permeabilization in 1% TritonX-100 (1 hour) before counting.

Analyses of free thiol groups

CoA and 3-bromopyruvate (BrPA) were prepared in PBS (pH 7.4), and *N*-acetyl cysteine (NAC) in water, and coincubated at room temperature (15 minutes). CoA and NAC alone were used as positive controls, and BrPA alone as a negative control. Solutions were added to black-walled 96-well plates with an equivalent volume of 10 μmol/L ThioGlo1 (Covalent Associates Inc.). Fluorescent signal was measured 5 minutes later at 379/513 nm.

Cytotoxicity assays

Cells were exposed to drugs for 48 to 72 hours, and viability was detected by addition of thiazoyl blue tetrazolium bromide (MTT) reagent. Formazan crystals were solubilized and absorbance read at 590/620 nm. Cell viability is displayed as a percentage of control cells, that is, cells with equivalent concentrations of the appropriate drug vehicle. Refer to Supplementary Material for detailed methods.

Cell viability and cycle analyses

Cells were stained with 7-aminoactinomycin D (7-AAD; 2 μg/mL) and Annexin V (AV). Viable (AV^-) and nonviable (AV^+) cell populations were determined by flow cytometry (BD FACSCanto I). For cell cycle, cells were permeabilized/stained with 0.4% Triton X-100, 2 μg/mL RNase, and 2 μmol/L TOPRO-3 in warm PBS. Profiles were determined by flow cytometry and sub-G_1 populations gated using FlowJo software (Tree Star Inc.).

Cell death assays

LDH release (LDH-Cytotoxicity Assay Kit II, Abcam) and caspase activity (Caspase-Glo 3/7 assay reagent, Promega) were measured by luminescence, as per manufacturer's instructions. DNA fragmentation was analyzed by agarose gel electrophoresis, as previously described (20).

Mass spectrometry

Cell samples (in ice-cold 6% perchloric acid) contained $^{13}C_3$-malonyl-CoA (0.5 μmol/L final) as an internal standard. Supernatants were loaded onto pre-equilibrated solid-phase extraction columns (Oasis HLB, 1 cc/30 mg, Waters) and dried eluates reconstituted in chromatography solvent. Analyses were performed using a triple quadrupole mass spectrometer (AB-Sciex 4000 Q-Trap) coupled to a Shimadzu LC-20AD LC system equipped with a Supelco Discovery C18 column (50 mm × 2.1 mm × 5 μm bead size).

Animal studies

Six-week-old female athymic nude mice (Crl:NU(NCr)-Foxn1^{nu}, Charles River Laboratories Inc.) were subcutaneously inoculated with 3×10^5 296 cells. Mice with palpable tumors (~2 mm diameter) were administered 2.5 mg/kg freshly prepared BrPA (pH 7.5) or equivalent volumes of PBS (vehicle) by intraperitoneal injection 4 days a week for 3 weeks. Mice were killed (CO_2 asphyxiation) when the largest tumor neared 1 cm^3. Tumor volumes (length × width^2/2) were calculated each week during treatment and at time of harvest. All animal experiments were approved by the University of Virginia Animal Care and Use Committee.

Statistical analysis

Unpaired 2-tailed Student *t* tests were used to determine the statistical differences between experimental and control groups where appropriate with $P < 0.05$ considered statistically significant. Pearson correlation coefficients (r and P values)

Published OnlineFirst September 9, 2014; DOI: 10.1158/0008-5472.CAN-14-0254

and linear regression graphs were derived from the GraphPad Prism program.

Results

Glucose transporters, and glycolytic and lipogenic enzymes, are upregulated in the malignant endometrium

We previously reported gene expression data from women with type I endometrial cancer who were matched for age (mean, 52.6 years) and BMI (mean, 44.5 kg/m^2; ref. 14). Mining the microarray data using gene set enrichment analysis identified the glycolysis and gluconeogenesis gene set as highly enriched in tumor-derived endometrium (NES, 1.87; $q = 0.02$; $P < 0.001$; Fig. 1A). Among the most elevated genes in malignant tissue were the glycolytic enzymes hexokinase 2 (*HK2*), glyceraldehyde-3-phosphate dehydrogenase (*GAPDH*), pyruvate kinase M2 (*PKM2*), and lactate dehydrogenase isoform A (*LDHA*; Fig. 1A). We also performed bioinformatics analyses on genes that were upregulated by more than 6-fold (371 genes) using the Database for Annotation, Visualization and Integrated Discovery (DAVID; refs. 21, 22) and matched these hits to the Panther biologic processes gene lists. These data identified that glycolytic and lipogenic metabolic pathways were enriched in malignant compared with nonmalignant endometrium (Fig. 1B). In an independent cohort of six patients with type I endometrial cancer, we validated the gene expression data at the protein level. Figure 1C shows the expression of glycolytic (HK2, PKM2, GAPDH, and LDHA) and DNL enzymes, including ATP citrate lyase (ACLY), acetyl-CoA carboxylases (ACC1 and ACC2), and fatty acid synthase (FASN). All of these enzymes except GAPDH were elevated in the majority of tumor versus adjacent nonmalignant tissue (Supplementary Fig. S1A).

Aberrations in the PTEN/PI3K/Akt pathway are common in type I endometrial cancer. In our samples, PTEN expression was reduced in one tumor sample, but activation of Akt (phosphorylation at Ser473) was evident in most tumor samples (Fig. 1D and Supplementary Fig. S1A). In contrast, the expression of PPARγ, glucose-6-phosphate dehydrogenase (G6PD), TSC2, and phosphorylation of p70 S6 ribosomal kinase (pS6K) were not dramatically altered between tumor and nontumor endometrial tissue (Supplementary Fig. S1B). Although alterations in LKB1 expression were observed in some tumors (Supplementary Fig. S1B), these changes were inconsistent between patient samples, that is, LKB1 expression was higher in one tumor and lower in other tumors, compared with adjacent nontumor tissue. Overall, these data indicate that Akt activation is associated with increased expression of glycolytic and lipogenic enzymes in endometrial tumor tissue (Supplementary Fig. S1A).

Glucose is a primary carbon source for glycolysis and lipogenesis and enters cells through glucose transporters. We manually ranked the GLUT family of transporters and identified GLUT6 (*SLC2A6*) as the 11th most upregulated gene overall and the most significantly elevated GLUT in the malignant endometrium (36.9-fold increase; Fig. 1E). Elevated GLUT6 protein expression was confirmed in tumor tissue compared with matched nontumor endometrium in five of the six patients (Fig. 1F and Supplementary Fig. S1A). GLUT6 is highly expressed in cancerous glandular epithelial cells, particularly those closest to blood vessels in the surrounding stroma (Fig. 1G and Supplementary Fig. S2). Blood vessels also stained positive for GLUT6. Glandular cells from the normal human endometrium had little or no expression of GLUT6 (Fig. 1G and Supplementary Fig. S2). In comparison, the ubiquitously expressed glucose transporter, GLUT1, was elevated by 4.3-fold at the gene level in the malignant endometrium (Fig. 1E) and in three of six tumors compared with nontumor endometrium (Fig. 1F and Supplementary Fig. S1A).

Analyses of TCGA datasets found that 40% of type I and 68% of type II endometrial cancers harbor alterations in the glycolytic–lipogenic gene set found in our cohort of patient samples (Table 1). The percentage of cases with alterations did not vary dramatically between women with stage I versus more advanced stages or lean versus obese within type I and within type II cancers (Table 1). However, patients with type I cancers (all cases) containing alterations in these genes had significantly poorer survival than those without gene alterations. Further examination of specific groups of type I cancers revealed poorer survival among obese women or those with stage II–IV cancers if they had the gene alterations (Table 1). Alterations in this gene set were also found in 80% of ovarian cancers. However, these genes were downregulated in a higher percentage of ovarian cancer cases (78 of 254, 30.7%) compared with type I (4 of 123, 3.25%) and type II (0/45, 0%) endometrial cancers and were not associated with worse survival (Table 1).

GLUT6 expression and glycolytic–lipogenic metabolism are upregulated in endometrial cancer cells

To further investigate endometrial cancer metabolism, we metabolically profiled seven human endometrial cancer cells, including HEC-1-A (HEC), Ishikawa (ISH), MFE-296 (296), MFE-319 (319), AN3CA (AN3), RL95-2 (RL), and KLE, and two immortalized cell lines derived from noncancerous endometrial tissue, MAD-11 (MAD) stromal and hUE-Ts (hUE) uterine epithelial cells. As shown in Fig. 2A, GLUT6 expression was upregulated in all seven endometrial cancer cells compared with noncancerous endometrial cells, whereas the expression of GLUT1 and all other glycolytic and DNL enzymes varied between cancer and noncancer cells (Fig. 2A and B). Akt was activated (phosphorylated) in the majority of cancerous endometrial cells, and PTEN expression was lost in three of the seven cancer cell lines (Fig. 2B).

To determine whether metabolic protein expression correlated with metabolism in endometrial cells, we measured oxygen consumption rate (OCR), extracellular acidification rate (ECAR), and macronutrient flux using radiolabeled glucose, glutamine, palmitate, and acetate tracers. Glycolysis, as measured by the conversion of tritiated glucose to tritiated water, was elevated in six of seven endometrial cancer cells compared with noncancerous endometrial cells (Fig. 2C and D), and glycolysis significantly correlated with ECAR ($r = 0.858$, $P = 0.003$; Fig. 2E). In contrast, glucose oxidation was markedly

Published OnlineFirst September 9, 2014; DOI: 10.1158/0008-5472.CAN-14-0254

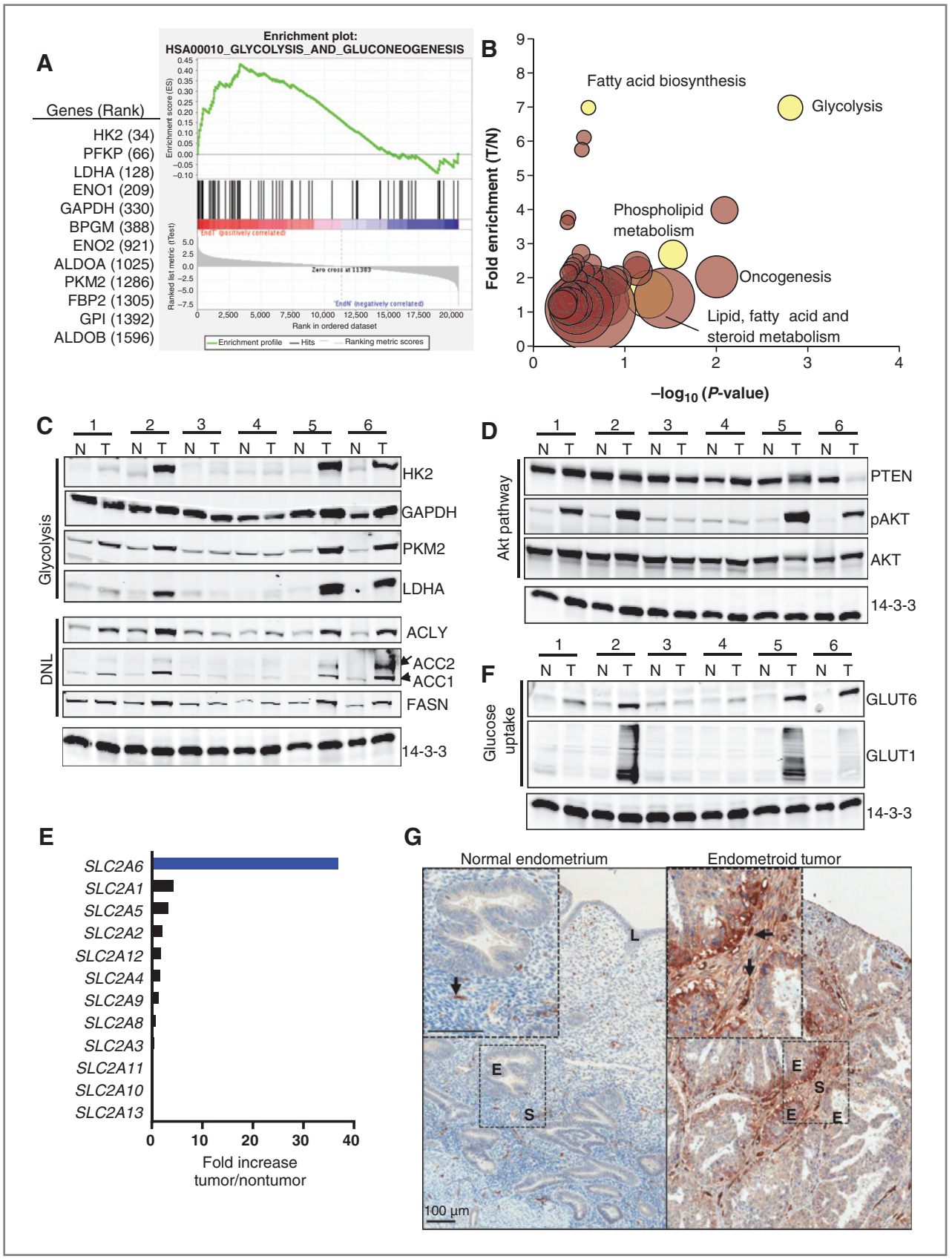

Published OnlineFirst September 9, 2014; DOI: 10.1158/0008-5472.CAN-14-0254

decreased in all seven endometrial cancer cells compared with the two noncancerous cells (Fig. 2F). The oxidation of glutamine (Fig. 2G) and palmitate (Fig. 2H) and OCR (Fig. 2I) was not associated with a cancer phenotype. Finally, DNL from glucose, glutamine, and acetate precursors was generally increased in most cancer-derived cells compared with noncancerous endometrial cells (Figs. 2J–L). Correlation analyses of these data revealed that GLUT6 protein expression significantly correlated with Warburg-type metabolism (low glucose oxidation/glycolysis ratio; $r = -0.837$, $P = 0.005$; Supplementary Fig. S3A), and the phosphorylation of Akt significantly correlated with glycolysis ($r = 0.849$, $P = 0.004$; Supplementary Fig. S3B) and glucose-derived lipogenesis in endometrial cells ($r = 0.777$, $P = 0.014$; Supplementary Fig. S3C).

GLUT6 promotes glycolysis and survival of endometrial cancer cells

Because GLUT6 has not been functionally characterized in cancer cells, we evaluated the role of GLUT6 using siRNA to knockdown this protein in 296 (Fig. 3A–I and Supplementary Fig. S4A–S4C) and RL cells (Supplementary Fig. S4D–S4H). Both of these cells were derived from type I endometrial tumors from postmenopausal Caucasian women, with the RL cells derived from an obese woman but the BMI is unknown for the source of the 296 cells (23, 24). SMARTpool (Pool) siRNA reduced GLUT6 protein expression in 296 cells by 65%, whereas siRNA sequence 4 (Seq.4; a single sequence from the SMARTpool) reduced GLUT6 protein expression by 90%, compared with controls (Fig. 3B and Supplementary Fig. S4A). Importantly, GLUT6 knockdown did not alter the expression of GLUT1, GLUT4, and GLUT8 (GLUT8 has the most sequence homology to GLUT6; ref. 25) in 296 cells (Supplementary Fig. S4B).

Functional analyses revealed that GLUT6 knockdown with the Pool siRNA reduced 296 and RL cell numbers by 62% and 59%, respectively, and with Seq.4 siRNA by 91% and 83%, respectively (Fig. 3C and Supplementary Fig. S4E, $P < 0.05$). Of note, GLUT6 knockdown with other individual siRNA sequences (shown in Supplementary Fig. S4A) also significantly reduced endometrial cancer cell numbers (data not shown). Cell loss induced by GLUT6 knockdown was due to cell death, as evidenced by morphologic alterations (Supplementary Fig. S4C), a marked increase in sub-G_1 populations (Fig. 3D and Supplementary Fig. S4F), number of AV^+ cells (Fig. 3E and Supplementary Fig. S4G), and release of LDH from permeabilized cells (Fig. 3F and Supplementary Fig. S4H).

To determine the role of GLUT6 in glucose metabolism, we measured glucose uptake and glycolysis in GLUT6 knockdown cells. Because complete knockdown of GLUT6 with Seq.4 siRNA induced significant cell death, the metabolism of 296 cells was investigated using the siRNA pool. Partial knockdown of GLUT6 expression significantly inhibited glucose uptake by 34% (Fig. 3G, $P = 0.001$), glycolysis by 33% (Fig. 3H, $P = 0.004$), and lactate release by 55% (Fig. 3I, $P < 0.001$).

Targeting metabolism in endometrial cancer cells

To test whether metabolic phenotypes could be exploited in endometrial cancer cells, we screened a panel of compounds known to target diverse metabolic pathways. Selectivity and toxicity of these compounds were compared with chemotherapeutics used to treat advanced-stage endometrial cancer. Endometrial cancer and noncancer cells displayed varying sensitivity to the DNA-damaging agent carboplatin (Fig. 4A). Notably, the noncancerous hUE cells were one of the most sensitive to carboplatin, compared with endometrial cancer and noncancerous MAD cells (Fig. 4A). In contrast, paclitaxel (a microtubule-stabilizing agent) showed greater selective toxicity toward endometrial cancer cells compared with noncancer cells (Fig. 4B). This sensitivity correlated with cell population doubling times, thereby validating the role microtubules play in cell division (Supplementary Fig. S5A and S5B; $r = 0.796$, $P = 0.01$).

Endometrial cells were then exposed to the glycolytic inhibitors 2-DG and BrPA (Fig. 4C and D), the lipogenesis inhibitor 5-(tetradecyloxy)-2-furoic acid (TOFA; Fig. 4E), the glucose oxidation agonist dichloroacetate (DCA; Fig. 4F), the fatty acid oxidation inhibitor etomoxir (Fig. 4G), the glucose and fatty acid uptake inhibitor, phloretin (Fig. 4H), the glutaminolysis inhibitor, 6-diazo-5-oxo-L-norleucine (DON; Fig. 4I), and the pleiotropic metabolic inhibitor, metformin (Fig. 4J). These compounds displayed a range of cytotoxic effects on the panel of endometrial cells including nonselective toxicity to all cells (e.g., 2-DG, metformin, and etomoxir), toxicity only at supraphysiologic concentrations (e.g., 2-DG and metformin), poor toxicity (e.g., DCA), or toxicity that plateaued with partial inhibition of cell viability (DON). However, as predicted by our metabolic flux data, TOFA was toxic to the cell lines with the highest rates of DNL and demonstrated mostly cancer cell–specific toxicity (Fig. 4E). Curiously, of all metabolic inhibitors, BrPA was the most disparately toxic between cell lines, with a 37-fold difference in sensitivity between the most sensitive (KLE, $IC_{50} = 34$ μmol/L) and the least sensitive cells (HEC, $IC_{50} = 1{,}267$ μmol/L; Fig. 4D). This suggested that sensitivity to BrPA was determined by specific cellular targets.

Figure 1. Glucose metabolism and DNL pathways are enriched in endometrial tumor tissue. A, enrichment plot of genes regulating glycolysis and gluconeogenesis in endometrial tumors compared with nontumor tissue. Glycolytic enzymes (ranked gene expression) are listed on the left. B, gene expression pathways enriched in the malignant endometrium compared with nontumor endometrium. Groups of genes regulating glycolysis, fatty acid biosynthesis, and lipid metabolism are depicted with yellow circles. Larger circle diameters indicate greater numbers of genes involved in pathway. C, D, and F, the expression of glycolytic/DNL enzymes, Akt signaling pathway proteins, and glucose transporters in tumor (T) and normal adjacent (N) endometrial tissue (six matched patient samples). 14-3-3 served as a loading control for all blots. E, fold increase in gene expression of GLUT transporter family members in endometrial tumor tissue compared with nontumor tissue. G, GLUT6 expression in tumor and normal endometrium. Endothelial (arrowheads), stromal (S), glandular epithelial (E), and luminal (L) cells of endometrium.

Published OnlineFirst September 9, 2014; DOI: 10.1158/0008-5472.CAN-14-0254

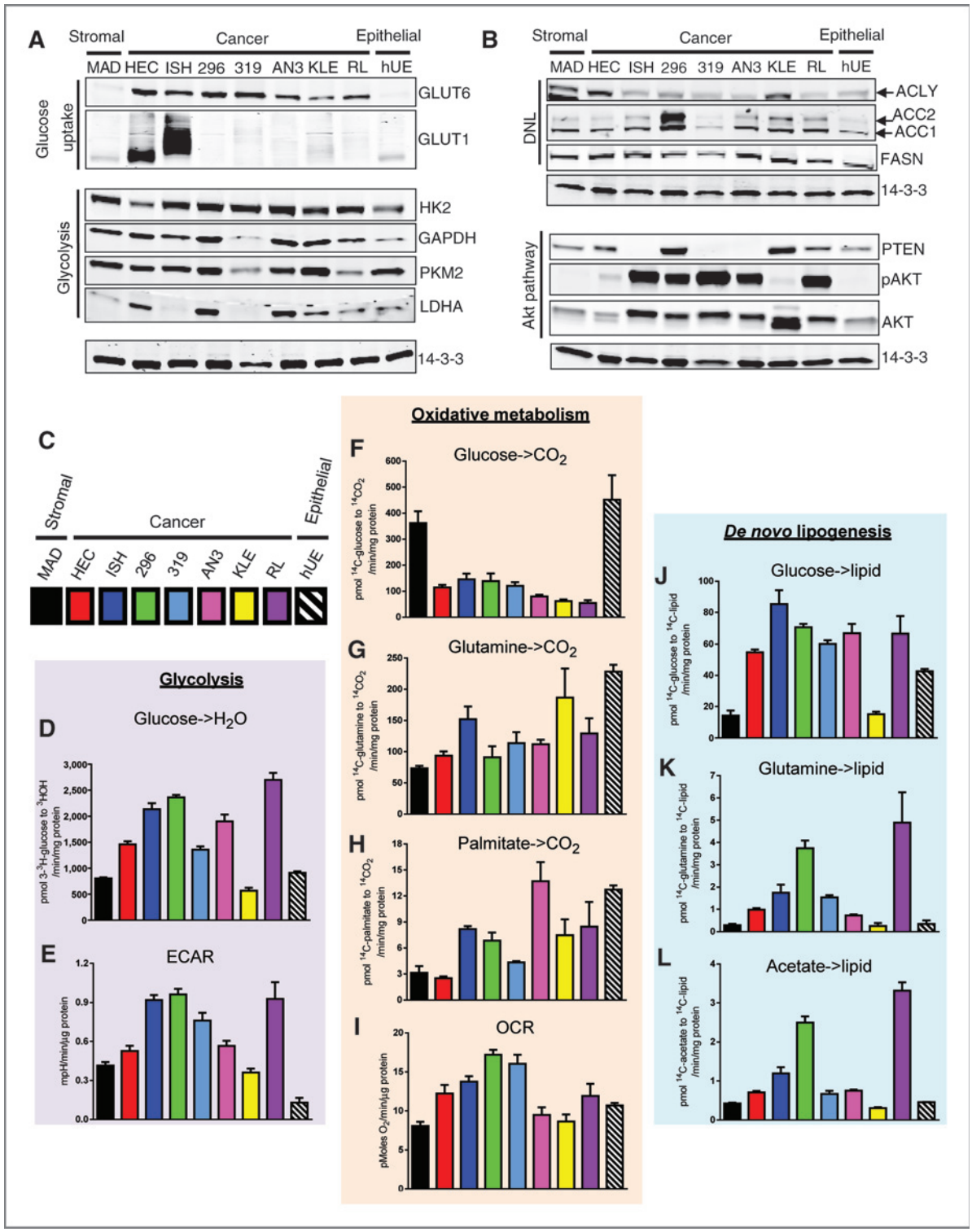

Figure 2. Cancerous endometrial cells display Warburg-like metabolism and elevated lipogenesis. Protein expression and metabolism of seven human endometrial cancer (*HEC, ISH, 296, 319, AN3, KLE, RL*) and noncancer stromal (*MAD*) and epithelial cells (*hUE*). A and B, glucose transporters, glycolytic/DNL enzymes, and Akt signaling pathway proteins in endometrial cells. 14-3-3 served as a loading control. C, boxes representing each cell line depicted in the following graphs. Glycolysis (D), ECAR (E), glucose oxidation (F), glutamine oxidation (G), palmitate oxidation (H), OCR (I), DNL from glucose (J), DNL from glutamine (K), and DNL from acetate (L) were measured for all cells. Metabolic assays represent the mean (±SEM) of three to five technical replicates (experiments were performed at least twice).

Published OnlineFirst September 9, 2014; DOI: 10.1158/0008-5472.CAN-14-0254

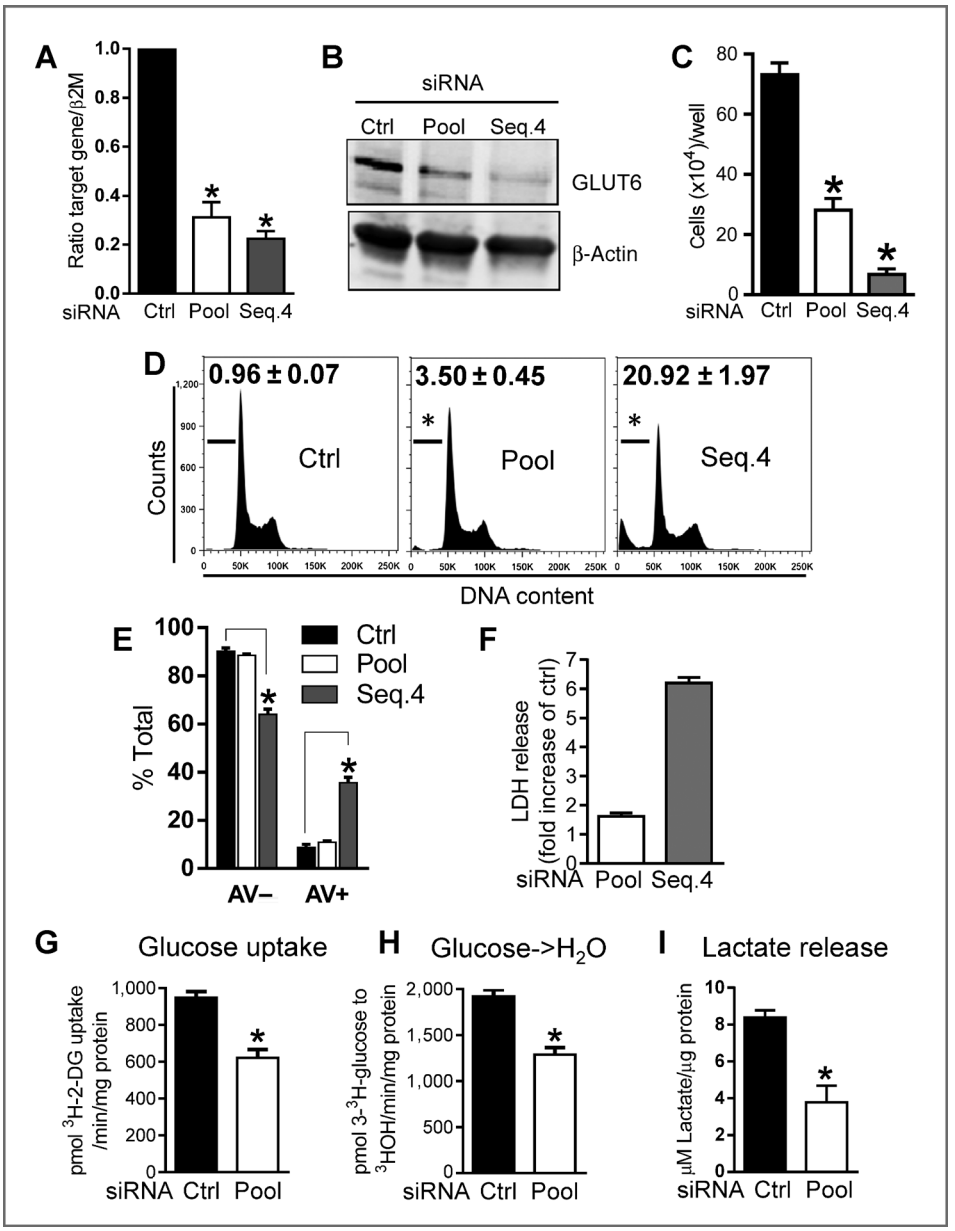

Figure 3. GLUT6 regulates glycolysis in endometrial cancer cells. A, GLUT6 mRNA expression was inhibited by 69% (Pool siRNA) and 78% (Seq.4 siRNA) in 296 cells, compared with controls (Ctrl siRNA) at 72 hours. B, GLUT6 protein expression was partially reduced by the siRNA Pool and inhibited by 90% with Seq.4 siRNA compared with controls at 96 hours. β-Actin served as loading control. C, GLUT6 knockdown with the siRNA Pool and Seq.4 significantly reduced 296 cell counts at 96 hours, compared with controls. D, cell-cycle analysis of siRNA-transfected 296 cells at 80 hours. Sub-G_1 populations (black bars) and population counts (% of total) are shown within histograms. E, AV^+ and AV^- 296 cells following GLUT6 siRNA transfection at 80 hours. Data are presented as percentage of total cells (positive and negative). F, LDH release in GLUT6 siRNA-transfected 296 cells (fold increase of control) at 96 hours. G, glucose uptake (^{3}H-2-DG) in siRNA-transfected 296 cells at 96 hours. H, glycolysis in siRNA-transfected 296 cells at 96 hours. I, lactate release into media from siRNA-transfected 296 cells at 72 hours (normalized to protein content per well). All data show the mean of at least three independent experiments ± SEM (*, $P < 0.05$). Time (h), time post-siRNA transfection.

BrPA inhibits DNL by pyruvylation of CoA

Birsoy and colleagues recently used BrPA in a global loss-of-function genetic screen to identify its selective cytotoxicity to glycolytic tumors. Their study demonstrated that BrPA requires monocarboxylate transporter 1 (MCT1) for transport into cells (26). Other studies have also shown that BrPA inhibits glycolysis by pyruvylation of GAPDH and HK2 (27). In evaluating the correlation between BrPA sensitivity and known cellular targets, we found that the expression of MCT1 (Supplementary Fig. S5C), HK2, and GAPDH (Fig. 2A), individually, did not correlate with sensitivity to BrPA (Supplementary Fig. S5D).

Glycolysis and lipogenesis were the two metabolic pathways most upregulated in endometrial tumors. We therefore investigated the effects of BrPA on these pathways in endometrial cancer cells. At a toxic dose (100 μmol/L), BrPA treatment inhibited glycolysis in 296 cells by 46% (Fig. 5A, $P < 0.0001$) but had a greater inhibitory effect on DNL from 3 different lipogenic precursors such as glucose (79% decrease, $P = 0.002$; Fig. 5B), glutamine (99% decrease, $P < 0.001$; Fig. 5C), and acetate (86% decrease, $P = 0.0002$; Fig. 5D). DNL from these precursors requires the production of acetyl-CoA. As BrPA inhibited DNL from acetate, which enters the lipogenic pathway as acetyl-CoA, we hypothesized that BrPA inhibited DNL at, or downstream of, acetyl-CoA production. Indeed, acetyl-CoA was depleted by 99% in BrPA-treated cells (Fig. 5E; $P < 0.002$). The formation of acetyl-CoA requires CoA. Because BrPA can pyruvylate free thiols (R-SH; ref. 28), we examined whether BrPA reacted with the thiol on CoA using a dye that fluoresces once bound to free thiol

Published OnlineFirst September 9, 2014; DOI: 10.1158/0008-5472.CAN-14-0254

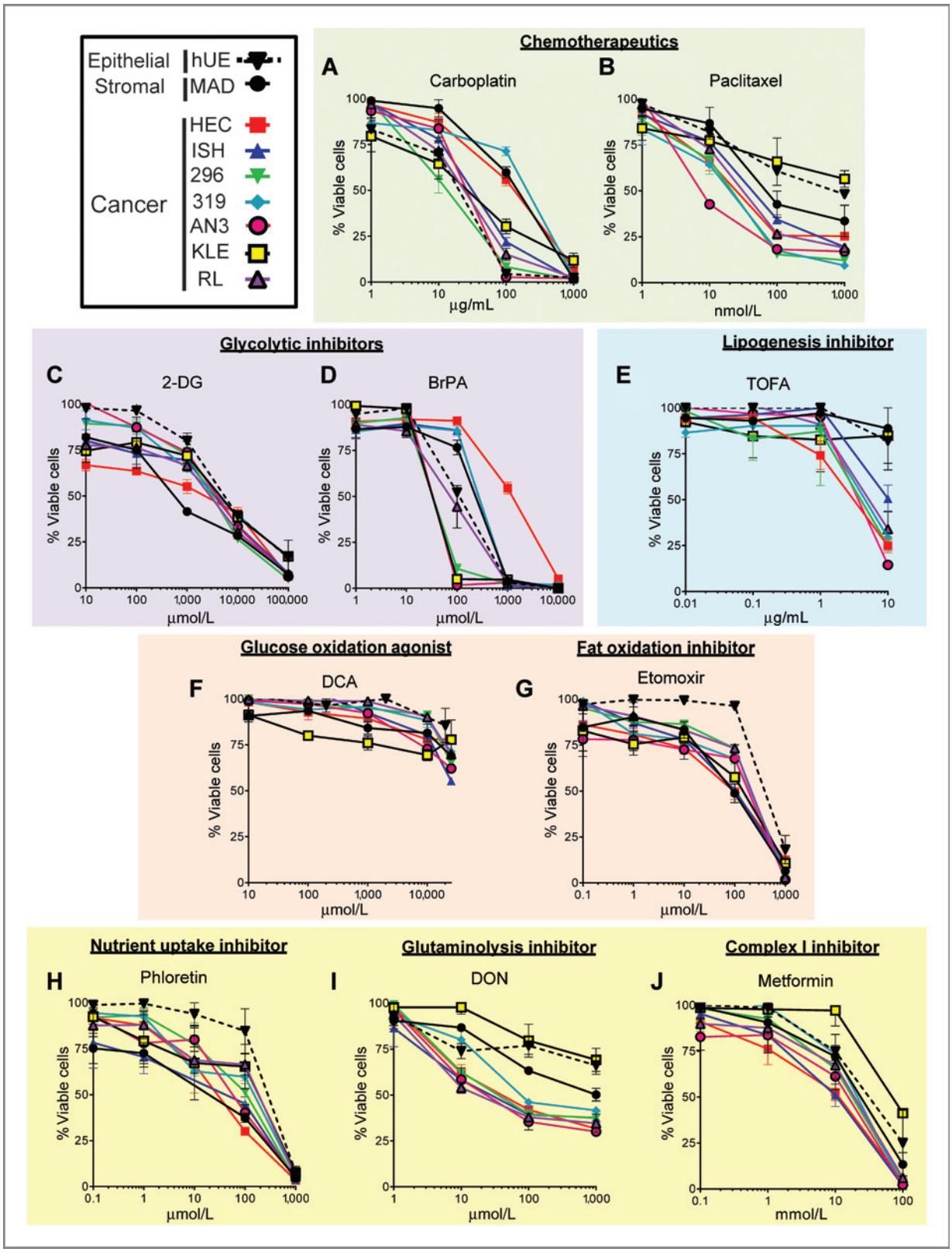

Figure 4. Sensitivity of endometrial cells to chemotherapeutics and compounds that target metabolism. Percentage viability of endometrial cancer (*HEC, ISH, 296, 319, AN3, KLE, RL)* and noncancer cells (*MAD, hUE*) following exposure to carboplatin (A), paclitaxel (B), 2-DG (C), BrPA (D), TOFA (E), DCA (F), etomoxir (G), phloretin (H), DON (I), and metformin (J). All dose–response curves represent the mean of 3 independent experiments. Error bars are ±SEM.

Published OnlineFirst September 9, 2014; DOI: 10.1158/0008-5472.CAN-14-0254

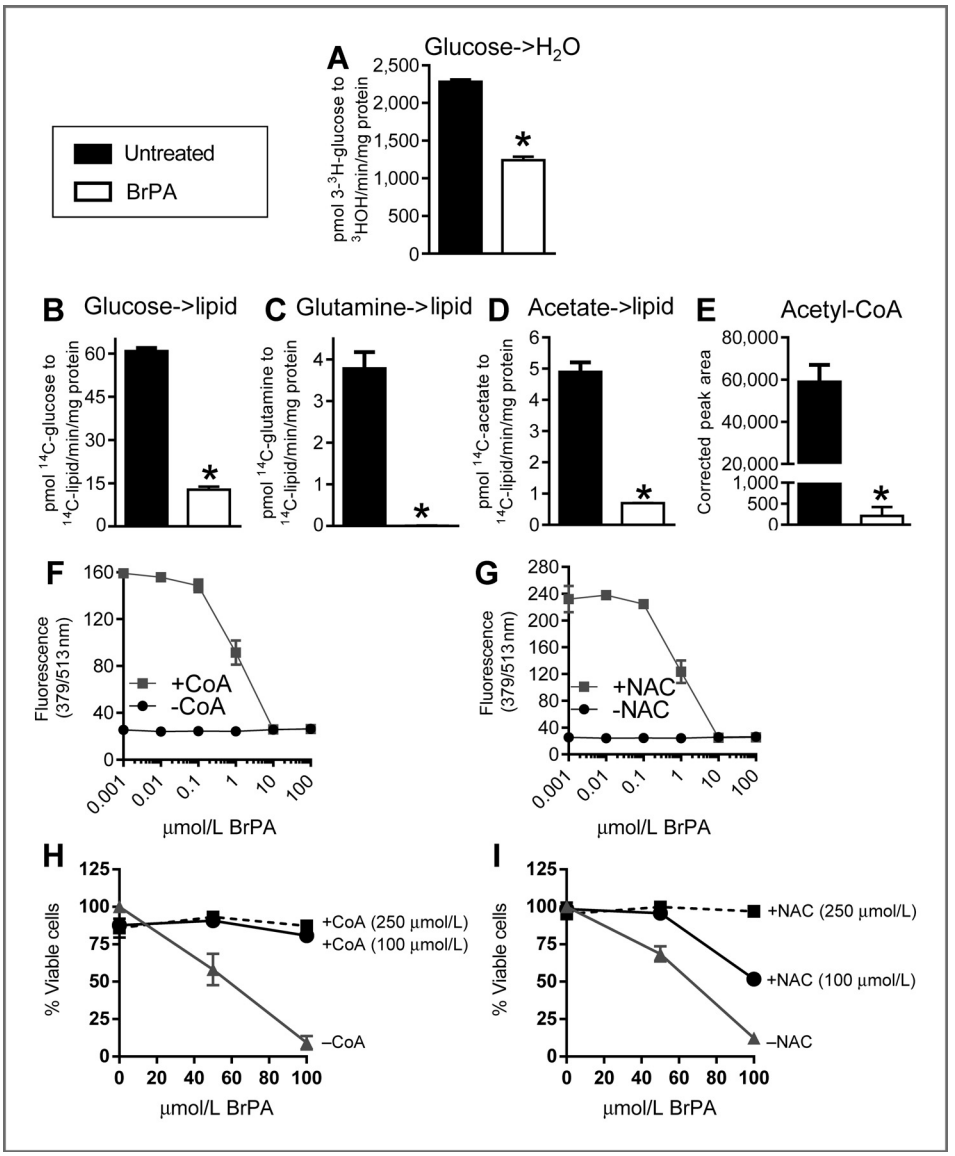

Figure 5. BrPA inhibits lipogenesis in endometrial cancer cells. A–D, glycolysis and substrate (glucose, glutamine, acetate) conversion to lipids were measured in 296 cells untreated or treated with 100 µmol/L BrPA (90 minutes). E, acetyl-CoA levels (corrected peak area) in 296 cells untreated or treated with 100 µmol/L BrPA for 90 minutes. F, activity of free thiol on CoA (1 µmol/L final reaction) was measured in presence of the indicated concentrations of BrPA (+CoA). G, activity of free thiol on NAC (1 µmol/L final reaction) was measured in presence of the indicated concentrations of BrPA (+NAC). BrPA without CoA or NAC are background controls (−CoA, −NAC). H and I, BrPA-mediated 296 cell death is rescued by pretreatment with CoA or NAC for 30 minutes. All metabolic assays and dose–response curves represent the mean (±SEM) of three independent experiments (*, $P < 0.05$).

groups (Fig. 5F). Co-incubation of BrPA with CoA at a 1:1 micromolar ratio inhibited fluorescent signal by 44% ($P < 0.001$) and a 10:1 micromolar ratio of BrPA to CoA completely inhibited fluorescent signal (Fig. 5F). These data indicated that BrPA was directly interfering with CoA at its free thiol group. Using a previously published ionization pattern for CoA (29), we demonstrated by mass spectrometry that pyruvylation occurs at the sulfhydryl group of CoA (Supplementary Fig. S6).

BrPA-mediated cytotoxicity is independent of reactive oxygen species generation

Previous studies have indicated that the antioxidant, NAC, protects against BrPA-mediated cell death by scavenging reactive oxygen species (ROS; ref. 30). Because NAC also harbors a thiol group, we postulated that NAC protects against BrPA-mediated cell death by binding to BrPA. Indeed, we found that co-incubation of BrPA with NAC at a 1:1 micromolar ratio inhibited fluorescent signal by 52% ($P < 0.001$) and a 10:1 micromolar ratio of BrPA to NAC completely inhibited fluorescent signal (Fig. 5G). These data suggested that BrPA-induced cell death may not be mediated by ROS. We therefore determined whether other antioxidants (without free thiols) could protect against BrPA-induced cell death. Indeed, although a toxic dose of BrPA increased ROS (Supplementary Fig. S7A and S7B), pretreatment of endometrial cancer cells with apocynin (Supplementary Fig. S7C), allopurinol (Supplementary Fig. S7D), *N* omega-nitro-L-arginine methyl ester (L-NAME; Supplementary Fig. S7E), manganese [III] tetrakis (4-benzoic acid) porphyrin (MnTBAP; Supplementary Fig. S7F), Mito-tempo (Supplementary Fig. S7G), resveratrol (Supplementary Fig. S7H), or ascorbic acid (Supplementary Fig. S7I) could not protect against BrPA-mediated cell death.

Published OnlineFirst September 9, 2014; DOI: 10.1158/0008-5472.CAN-14-0254

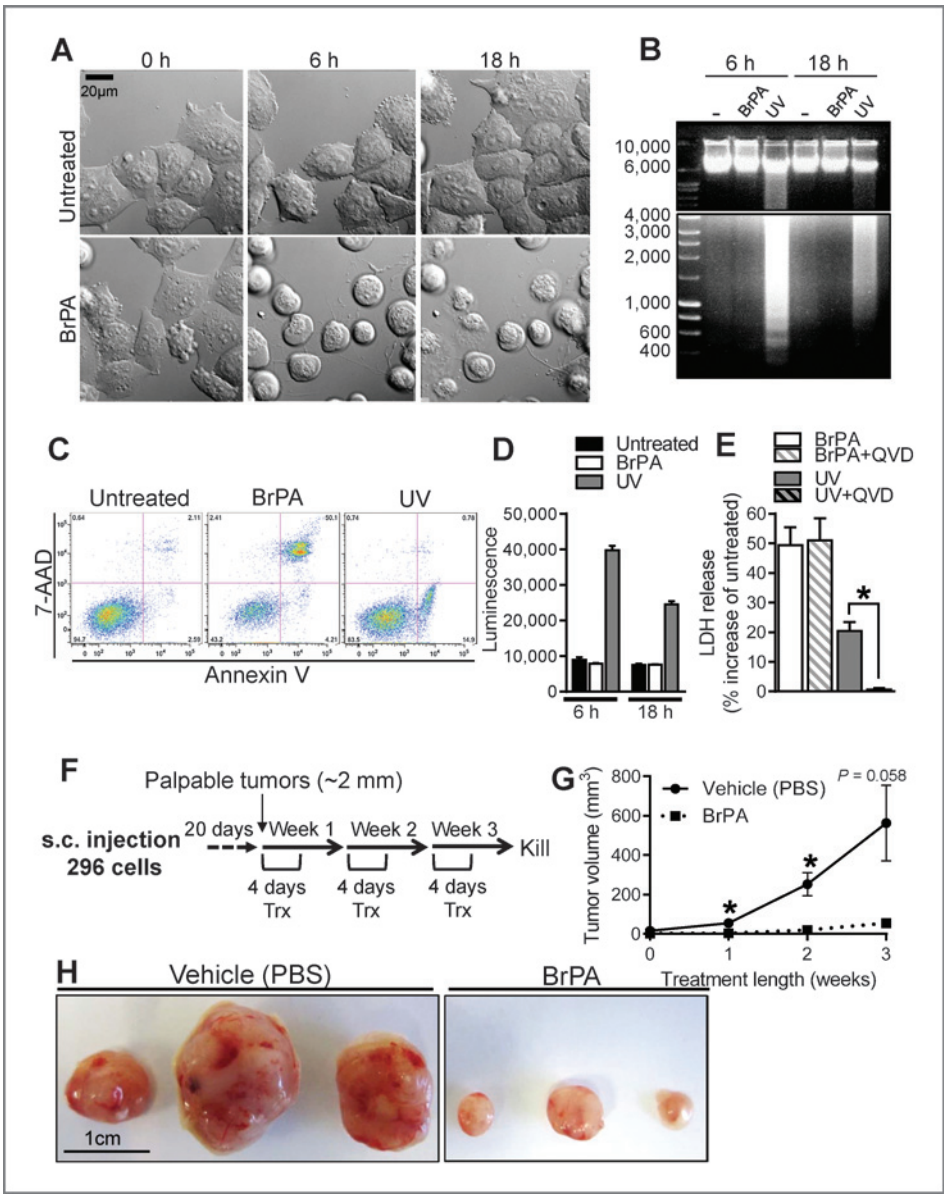

Figure 6. BrPA induces necrosis and impairs endometrial tumor growth *in vivo*. A, phase contrast images of 296 cells, untreated or treated, with BrPA (100 μmol/L). B, DNA fragmentation in untreated, BrPA-treated, or UV-irradiated (150,000 μJoules/cm^2) 296 cells. C, AV/7-AAD staining of 296 cells following BrPA treatment or UV irradiation (24-hour BrPA treatment, 5-hour after UV irradiation). D, caspase-3/7 activity in 296 cells following BrPA treatment or UV irradiation. E, LDH release in 296 cells treated with BrPA (±QVD) or UV-irradiated (±QVD; 18 hours posttreatment). LDH release is calculated as a percentage increase of untreated cells. All *in vitro* data represent the mean of at least three independent experiments ± SEM. F, schematic of BrPA dosing in mice. G, growth of 296 tumors in mice treated with vehicle or BrPA (2.5 mg/kg; $n = 3$). Data points represent the mean tumor volume ± SEM. H, 296 tumors from mice treated with vehicle (PBS) or BrPA (*, $P < 0.05$).

Because other antioxidants could not protect against BrPA-induced cell death, we proposed that excess CoA and NAC could act as "sponges" to react with BrPA and prevent cytotoxicity. Indeed, pretreatment of 296 cells with CoA (Fig. 5H) and NAC (Fig. 5I) protected from BrPA-induced death. Similar results were reproduced in RL cells (data not shown).

BrPA induces necrosis *in vitro* and inhibits endometrial tumor growth *in vivo*

BrPA inhibits glycolytic–lipogenic metabolism and depletes intracellular ATP (60% decrease at 1.5 hours, $P < 0.0001$; Supplementary Fig. S8A). These alterations can induce cell death by multiple mechanisms. Using UV irradiation as a positive control, we evaluated the effects of BrPA on classic features of apoptosis. Treatment of 296 cells with BrPA did not induce dynamic membrane blebbing (BrPA-treated cells are shown in Fig. 6A and UV-irradiated cells in Supplementary Fig. S8B), DNA fragmentation (Fig. 6B), an increase in apoptotic cell populations (AV$^+$/7-AAD negative; Fig. 6C), or activation of caspases (Fig. 6D). Furthermore, BrPA-mediated cell death was associated with an increase in LDH release, and this was not prevented by the pan-caspase inhibitor, Q-VD-OPH (QVD; Fig. 6E and Supplementary Fig. S8C). From these observations, we conclude that BrPA-mediated cell death was due to necrosis. Because BrPA kills endometrial cancer cells *in vitro*, we tested the efficacy of this agent against endometrial tumors *in vivo*. BrPA (2.5 mg/kg) or vehicle (PBS) was administered to nude mice with palpable 296 tumors (Fig. 6F). As a single agent, BrPA dramatically inhibited tumor growth compared with vehicle controls (Fig. 6G and H).

Published OnlineFirst September 9, 2014; DOI: 10.1158/0008-5472.CAN-14-0254

Discussion

Increased glucose metabolism (glycolysis) and flux through lipogenesis is a hallmark feature of many cancers, providing structural molecules and aiding intracellular signaling and transport that is required for cancer progression (31). Analyses of TCGA data sets found that 40% to 68% of endometrial cancers (type I and II) harbor alterations in the glycolytic–lipogenic genes that we observed in our cohort of patient samples. Interestingly, only women with type I tumors who had these alterations (including those with stages II–IV and obese patients) had worse overall survival than those without. In contrast, in ovarian cancer (a malignancy not typically associated with obesity), alterations in these genes were more common (80% of cases) but were more frequently downregulated and not associated with survival. While it is clear that alterations in genes controlling glycolytic–lipogenic processes are not unique to endometrial cancer, this metabolic pathway appears to impact the outcome of treatment and/or disease progression in women with type I endometrial cancer. Therefore, therapeutic targeting of this pathway may improve survival rates for these subsets of patients.

Facilitative glucose uptake feeds glycolytic–lipogenic metabolism and is regulated by the GLUT family (GLUTs 1–14). Many of these are expressed in the uterus and some, including the ubiquitously expressed GLUT1, are elevated in endometrial cancer (25, 32–35). GLUT1 is thought to contribute to basal glucose uptake in normal tissues, and upregulation of this transporter has been reported in many malignancies (36). In this study, GLUT1 expression was only increased in some of our patient tumor samples and it was not specific to cancerous endometrial cells. In contrast, GLUT6 was the most elevated glucose transporter in malignant endometrial tissue and it was the only protein specifically upregulated in endometrial cancer cells. Furthermore, we demonstrated that GLUT6 promotes glycolysis and survival of endometrial cancer cells, despite the expression of other glucose transporters. These data suggest that either endometrial cancer cells become dependent on glucose uptake via GLUT6 or GLUT6 may have other roles in cancer biology that remain to be discovered.

Metabolic profiling of endometrial cancer cells showed higher rates of glycolysis and lower glucose oxidation than their nonmalignant counterparts. However, oxidative metabolism in general was not defective in endometrial cancer cells. Our results suggest that glucose oxidation is specifically decreased in endometrial cancer cells by a mechanism that is independent of a dysfunction in mitochondrial tricarboxylic acid (TCA) cycle or oxidative phosphorylation machinery. Furthermore, our data support the concept that glucose-derived carbons are preferentially used by cancer cells for macromolecule synthesis to promote cell proliferation (37, 38). Constitutive activation of the PI3K/Akt pathway in cancer cells is thought to contribute to this metabolic phenotype by stimulating glucose transport and metabolism. In our study, activation of Akt was associated with increased glycolytic–lipogenic metabolism in endometrial cancer cells. Activation of Akt also influences protein synthesis through mTOR, and alterations in this pathway have been reported in endometrial cancer (13, 39). However, in our cohort of patients, we found that TSC2 expression (negative regulator of mTOR) and the phosphorylation of S6K1 (an mTOR target that regulates protein synthesis) were similar in endometrial tumor versus adjacent nontumor tissue. Together, our data provide support for Akt activation as a central regulator of glycolytic–lipogenic metabolism in cancer cells.

In recent years, a number of studies have reported the anticancer activity of BrPA (26, 27, 40–46), and a modified formula of BrPA was effective at reducing the growth of advanced hepatocellular carcinoma in a human patient (28). However, the metabolic consequences, molecular targets, and mechanism of action for this agent remain unclear. In endometrial cells, it appears that sensitivity to BrPA is not solely mediated by the expression of an individual protein. We also found that BrPA is a potent inhibitor of lipogenesis, by depleting the lipid precursor acetyl-CoA. Other studies have reported that BrPA lowers acetyl-CoA levels in noncancer cells (47, 48), although our study is the first to report that the mechanism for acetyl-CoA depletion is due to pyruvylation of CoA. CoA is an important cofactor for intermediary nutrient metabolism and is thought to be involved in up to 4% of all cellular enzymatic reactions (49). Therefore, BrPA has the ability to alter numerous metabolic reactions by pyruvylating thiols, including that of the intracellular reducing agent glutathione (GSH), as proposed earlier (40, 50). GSH is important for protecting cells against ROS, and it has been suggested that BrPA-mediated cell death is due to oxidative stress (30). However, in this study, BrPA-induced cell death was not protected by any antioxidant except the thiol-containing NAC. We therefore propose that BrPA-induced cell death is not due to increased ROS generation at least in endometrial cancer cells.

Overall, this study supports an important role for glucose metabolism in endometrial tumor growth. More specifically, endometrial cancer cells may rely on GLUT6-mediated glucose transport and glycolytic–lipogenic metabolism for survival and these features represent vulnerabilities that are amenable to therapeutic intervention. BrPA may prove useful to treat endometrial cancer because it is a dual glycolytic–lipogenic inhibitor. However, the pleiotropic effects of this agent may limit its administration for anticancer therapy. As such, a modified formula or targeted delivery of BrPA to tumors may be required to reduce off-target toxicity. From a clinical standpoint, our data suggest that maintenance of blood glucose levels by regulation of dietary intake and/or administration of hypoglycemic agents may be helpful at reducing the growth of endometrial tumors. Future studies are required to delineate the role of glucose availability and metabolism in the etiology of endometrial cancer.

Disclosure of Potential Conflicts of Interest

J.M. Lancaster received speakers' bureau honoraria from Amgen. No potential conflicts of interest were disclosed by the other authors.

Published OnlineFirst September 9, 2014; DOI: 10.1158/0008-5472.CAN-14-0254

Authors' Contributions

Conception and design: F.L. Byrne, S.C. Modesitt, J.M. Lancaster, J.K. Slack-Davis, K.L. Hoehn

Development of methodology: F.L. Byrne, I.K.H. Poon, J.L. Tomsig, K.S. Ravichandran, K.L. Hoehn

Acquisition of data (provided animals, acquired and managed patients, provided facilities, etc.): F.L. Byrne, I.K.H. Poon, J.L. Tomsig, J.D.Y. Chow, M.E. Healy, W.D. Baker, J.M. Lancaster, K.S. Ravichandran, K.L. Hoehn

Analysis and interpretation of data (e.g., statistical analysis, biostatistics, computational analysis): F.L. Byrne, I.K.H. Poon, W.D. Baker, K. Atkins, K.S. Ravichandran, K.L. Hoehn

Writing, review, and/or revision of the manuscript: F.L. Byrne, S.C. Modesitt, K. Atkins, J.M. Lancaster, K.H. Moley, J.K. Slack-Davis, K.L. Hoehn

Administrative, technical, or material support (i.e., reporting or organizing data, constructing databases): F.L. Byrne, D.C. Marchion, K.L. Hoehn

Study supervision: F.L. Byrne, K.H. Moley, K.L. Hoehn

Acknowledgments

The authors thank Dr. Sarah Parsons, the Women's Oncology group at the University of Virginia, members of the Hoehn, Slack-Davis, and Parsons Laboratories, and Amanda Watson for helpful discussions. We thank Dr. Carl Creutz (University of Virginia) for assistance with the detection of free thiols.

Grant Support

This research was funded through the Department of Pharmacology start-up funds (K.L. Hoehn), by the UVA Cancer Center Pilot Award through the Women's Oncology Research Fund and the NCI Cancer Center Support Grant P30-CA44579 (S.C. Modesitt, J.K. Slack-Davis, and K.L. Hoehn). F.L. Byrne is a Hope Funds for Cancer Research Fellow supported by the Hope Funds for Cancer Research (HFCR-14-06-04).

The costs of publication of this article were defrayed in part by the payment of page charges. This article must therefore be hereby marked *advertisement* in accordance with 18 U.S.C. Section 1734 solely to indicate this fact.

Received January 29, 2014; revised July 28, 2014; accepted August 13, 2014; published OnlineFirst September 9, 2014.

References

1. Ferlay J, Shin H-R, Bray F, Forman D, Mathers C, Parkin DM. Estimates of worldwide burden of cancer in 2008: GLOBOCAN 2008. Int J Cancer 2010;127:2893–2917.
2. Barlin JN, Wysham WZ, Ferda AM, Khoury-Collado F, Cassella DK, Alektiar KM, et al. Location of disease in patients who die from endometrial cancer: a study of 414 patients from a single institution. Int J Gynecol Cancer 2012;22:1527–31.
3. Felix AS, Weissfeld JL, Stone RA, Bowser R, Chivukula M, Edwards RP, et al. Factors associated with Type I and Type II endometrial cancer. Cancer Causes Control 2010;21:1851–6.
4. Weigelt B, Banerjee S. Molecular targets and targeted therapeutics in endometrial cancer. Curr Opin Oncol 2012;24:554–63.
5. Calle EE, Kaaks R. Overweight, obesity and cancer: epidemiological evidence and proposed mechanisms. Nat Rev Cancer 2004;4:579–591.
6. Calle EE, Rodriguez C, Walker-Thurmond K, Thun MJ. Overweight, obesity, and mortality from cancer in a prospectively studied cohort of U.S. adults. N Engl J Med 2003;348:1625–38.
7. McCawley GM, Ferriss JS, Geffel D, Northup CJ, Modesitt SC. Cancer in obese women: potential protective impact of bariatric surgery. J Am Coll Surg 2009;208:1093–8.
8. Lambe M, Wigertz A, Garmo H, Walldius G, Jungner I, Hammar N. Impaired glucose metabolism and diabetes and the risk of breast, endometrial, and ovarian cancer. Cancer Causes Control 2011;22:1163–1171.
9. Zendehdel K, Nyren O, Ostenson CG, Adami HO, Ekbom A, Ye W. Cancer incidence in patients with type 1 diabetes mellitus: a population-based cohort study in Sweden. J Natl Cancer Inst 2003;95:1797–800.
10. Modesitt SC, Geffel DL, Via J, Weltman LA. Morbidly obese women with and without endometrial cancer: are there differences in measured physical fitness, body composition, or hormones? Gynecol Oncol 2012;124:431–6.
11. Kandoth C, Schultz N, Cherniack AD, Akbani R, Liu Y, Shen H, et al. Integrated genomic characterization of endometrial carcinoma. Nature 2013;497:67–73.
12. Contreras CM, Gurumurthy S, Haynie JM, Shirley LJ, Akbay EA, Wingo SN, et al. Loss of Lkb1 provokes highly invasive endometrial adenocarcinomas. Cancer Res 2008;68:759–66.
13. Lu KH, Wu W, Dave B, Slomovitz BM, Burke TW, Munsell MF, et al. Loss of tuberous sclerosis complex-2 function and activation of mammalian target of rapamycin signaling in endometrial carcinoma. Clin Cancer Res 2008;14:2543–50.
14. Modesitt SC, Hsu JY, Chowbina SR, Lawrence RT, Hoehn KL. Not all fat is equal: differential gene expression and potential therapeutic targets in subcutaneous adipose, visceral adipose, and endometrium of obese women with and without endometrial cancer. Int J Gynecol Cancer 2012;22:732–41.
15. Cerami E, Gao J, Dogrusoz U, Gross BE, Sumer SO, Aksoy BA, et al. The cBio cancer genomics portal: an open platform for exploring multidimensional cancer genomics data. Cancer Discov 2012;2:401–4.
16. Gao J, Aksoy BA, Dogrusoz U, Dresdner G, Gross B, Sumer SO, et al. Integrative analysis of complex cancer genomics and clinical profiles using the cBioPortal. Sci Signal 2013;6:pl1.
17. Bell D, Berchuck A, Birrer M, Chien J, Cramer DW, Dao F, et al. Integrated genomic analyses of ovarian carcinoma. Nature 2011;474:609–615.
18. cancergenome.nih.gov [Internet]. Maryland: The Cancer Genome Atlas (TCGA) Research Network; 2014 [updated 2014; cited 2014 Jul 25]. Available from http://cancergenome.nih.gov.
19. Pfaffl MW. A new mathematical model for relative quantification in real-time RT-PCR. Nucleic Acids Res 2001;29:e45.
20. Kasibhatla S, Amarante-Mendes GP, Finucane D, Brunner T, Bossy-Wetzel E, Green DR. Analysis of DNA fragmentation using agarose gel electrophoresis. Cold Spring Harbor Protocols 2006;2006:pdb.prot4429.
21. Huang DW, Sherman BT, Lempicki RA. Systematic and integrative analysis of large gene lists using DAVID bioinformatics resources. Nat Protocols 2008;4:44–57.
22. Huang DW, Sherman BT, Lempicki RA. Bioinformatics enrichment tools: paths toward the comprehensive functional analysis of large gene lists. Nucleic Acids Res 2009;37:1–13.
23. Hackenberg R, Beck S, Filmer A, Hushmand Nia A, Kunzmann R, Koch M, et al. Androgen responsiveness of the new human endometrial cancer cell line MFE-296. Int J Cancer 1994;57:117–22.
24. Way DL, Grosso DS, Davis JR, Surwit EA, Christian CD. Characterization of a new human endometrial carcinoma (RL95–2) established in tissue culture. In Vitro 1983;19:147–58.
25. Doege H, Bocianski A, Joost HG, Schurmann A. Activity and genomic organization of human glucose transporter 9 (GLUT9), a novel member of the family of sugar-transport facilitators predominantly expressed in brain and leucocytes. Biochem J 2000;350:771–6.
26. Birsoy K, Wang T, Possemato R, Yilmaz OH, Koch CE, Chen WW, et al. MCT1-mediated transport of a toxic molecule is an effective strategy for targeting glycolytic tumors. Nat Genet 2013;45:104–108.
27. Ganapathy-Kanniappan S, Kunjithapatham R, Geschwind J-FH. Anticancer efficacy of the metabolic blocker 3-bromopyruvate: specific molecular targeting. Anticancer Res 2013;33:13–20.
28. Ko YH, Verhoeven HA, Lee MJ, Corbin DJ, Vogl TJ, Pedersen PL. A translational study "case report" on the small molecule "energy blocker" 3-bromopyruvate (3BP) as a potent anticancer agent: from bench side to bedside. J Bioenerg Biomembr 2012;44:163–70.
29. Burns KL, Gelbaum LT, Sullards MC, Bostwick DE, May SW. Isocoenzyme A. J Biol Chem 2005;280:16550–8.
30. Kim JS, Ahn KJ, Kim JA, Kim HM, Lee JD, Lee JM, et al. Role of reactive oxygen species-mediated mitochondrial dysregulation in 3-bromopyruvate induced cell death in hepatoma cells: ROS-mediated cell death by 3-BrPA. J Bioenerg Biomembr 2008;40:607–18.
31. Menendez JA, Lupu R. Fatty acid synthase and the lipogenic phenotype in cancer pathogenesis. Nat Rev Cancer 2007;7:763–777.

Published OnlineFirst September 9, 2014; DOI: 10.1158/0008-5472.CAN-14-0254

32. Frolova AI, Moley KH. Glucose transporters in the uterus: an analysis of tissue distribution and proposed physiological roles. Reproduction 2011;142:211–20.
33. Goldman NA, Katz EB, Glenn AS, Weldon RH, Jones JG, Lynch U, et al. GLUT1 and GLUT8 in endometrium and endometrial adenocarcinoma. Mod Pathol 2006;19:1429–36.
34. Knapp P, Chabowski A, Harasiuk D, Gorski J. Reversed glucose and fatty acids transporter expression in human endometrial cancer. Horm Metab Res 2012;44:436–41.
35. Krzeslak A, Wojcik-Krowiranda K, Forma E, Jozwiak P, Romanowicz H, Bienkiewicz A, et al. Expression of GLUT1 and GLUT3 glucose transporters in endometrial and breast cancers. Pathol Oncol Res 2012;18:721–8.
36. Macheda ML, Rogers S, Best JD. Molecular and cellular regulation of glucose transporter (GLUT) proteins in cancer. J Cell Physiol 2005; 202:654–62.
37. Vander Heiden MG, Cantley LC, Thompson CB. Understanding the warburg effect: the metabolic requirements of cell proliferation. Science 2009;324:1029–33.
38. Ward Patrick S, Thompson Craig B. Metabolic reprogramming: a cancer hallmark even warburg did not anticipate. Cancer Cell 2012;21: 297–308.
39. Slomovitz BM, Coleman RL. The PI3K/AKT/mTOR pathway as a therapeutic target in endometrial cancer. Clin Cancer Res 2012;18: 5856–64.
40. Calvino E, Estan MC, Sanchez-Martin C, Brea R, de Blas E, Boyano-Adanez MC, et al. Regulation of death induction and chemosensitizing action of 3-bromopyruvate in myeloid leukemia cells. energy depletion, oxidative stress, protein kinase activity modulation. J Pharmacol Exp Ther 2013;348:324–35.
41. Cardaci S, Rizza S, Filomeni G, Bernardini R, Bertocchi F, Mattei M, et al. Glutamine deprivation enhances antitumor activity of 3-bromopyruvate through the stabilization of monocarboxylate transporter-1. Cancer Res 2012;72:4526–36.
42. Kim W, Yoon J-H, Jeong J-M, Cheon G-J, Lee T-S, Yang J-I, et al. Apoptosis-inducing antitumor efficacy of hexokinase II inhibitor in hepatocellular carcinoma. Mol Cancer Ther 2007;6:2554–62.
43. Tang Z, Yuan S, Hu Y, Zhang H, Wu W, Zeng Z, et al. Over-expression of GAPDH in human colorectal carcinoma as a preferred target of 3-bromopyruvate propyl ester. J Bioenerg Biomembr 2012;44:117–25.
44. Thangaraju M, Karunakaran SK, Itagaki S, Gopal E, Elangovan S, Prasad PD, et al. Transport by SLC5A8 with subsequent inhibition of histone deacetylase 1 (HDAC1) and HDAC3 underlies the antitumor activity of 3-bromopyruvate. Cancer 2009;115: 4655–66.
45. Zhang Q, Pan J, North PE, Yang S, Lubet RA, Wang Y, et al. Aerosolized 3-bromopyruvate inhibits lung tumorigenesis without causing liver toxicity. Cancer Prev Res 2012;5:717–25.
46. Zhang X, Varin E, Briand M, Allouche S, Heutte N, Schwartz L, et al. Novel therapy for malignant pleural mesothelioma based on anti-energetic effect: an experimental study using 3-Bromopyruvate on nude mice. Anticancer Res 2009;29:1443–8.
47. Bielarczyk H, Szutowicz A. Evidence for the regulatory function of synaptoplasmic acetyl-CoA in acetylcholine synthesis in nerve endings. Biochem J 1989;262:377–80.
48. Ricny J, Tucek S. Acetyl coenzyme A and acetylcholine in slices of rat caudate nuclei incubated in the presence of metabolic inhibitors. J Biol Chem 1981;256:4919–23.
49. Leonardi R, Zhang Y-M, Rock CO, Jackowski S. Coenzyme A: back in action. Prog Lipid Res 2005;44:125–153.
50. Qin JZ, Xin H, Nickoloff BJ. 3-Bromopyruvate induces necrotic cell death in sensitive melanoma cell lines. Biochem Biophys Res Commun 2010;396:495–500.

Supplemental Methods

Targets/functions of metabolic drugs and antioxidants

2-DG (non-metabolizable glucose analog), TOFA (ACC inhibitor), DCA (pyruvate dehydrogenase kinase inhibitor), etomoxir (a carnitine palmitoyltransferase I inhibitor) DON (amino acid that inhibits glutaminase and other glutamine metabolizing enzymes), metformin (targets mitochondrial complex I), apocynin (a NADPH oxidase inhibitor), allopurinol (a xanthine oxidoreductase inhibitor) L-NAME (a nitric oxide synthase inhibitor), manganese [III] tetrakis (4-benzoic acid) porphyrin, MnTBAP (superoxide dismutase mimetic and peroxynitrite inhibitor), 2-(2,2,6,6-Tetramethylpiperidin-1-oxyl-4-ylamino)-2-oxoethyl)triphenylphosphonium chloride . monohydrate, Mito-TEMPO (mitochondrial superoxide and alkyl radical scavenger), and resveratrol (cyclooxygenase-1 inhibitor).

Preparation of protein lysates

Cells were sonicated, and frozen endometrial tissue homogenized, in radio-immunoprecipitation assay (RIPA) buffer [150mM NaCl, 10mmol/L nonyl phenoxypolyethoxylethanol (NP)-40, 0.5% sodium deoxycholate, 0.1% sodium dodecyl sulphate (SDS), 50mmol/L Tris pH 7.5] containing protease inhibitors (Thermo Scientific Pierce, Rockford, IL, USA) and phosphatase inhibitors (2mM Na-orthovanadate, 1mM Na-pyrophosphate, 10mM Na-fluoride, 250nM microcystin LR). Cellular proteins (20µg) were resolved on AnykD pre-cast gels (Bio-Rad Laboratories, Hercules, CA) or 10% SDS-polyacrylamide gels.

Nutrient metabolism assays

Sub-confluent cells were incubated in Krebs Ringer Phosphate (KRP) solution with nutrients (120mM NaCl, 600µM Na_2HPO_4, 400µM NaH_2PO_4, 6mM KCl, 1.2mM $MgSO_4$, 12.5mM HEPES pH 7.4, 1mM $CaCl_2$, 5mM glucose, 500µM glutamine, 125µM palmitate, 50µM acetate, 1mM L-carnitine, 0.25% fatty acid-free BSA) containing either 10µCi/mL D-[3-^{3}H]glucose, 5µCi/mL D-[^{14}C(U)] glucose, 1µCi/mL L[^{14}C(U)]-glutamic acid, 2µCi/mL[1-^{14}C]-palmitic acid, or 10µCi/mL [2-^{14}C] acetic acid sodium salt for 90 minutes in sealed wells. For BrPA treatment, 100x concentrated drug was prepared in KRP (pH 7.5) and added to each well at the indicated concentrations. Substrate oxidation was measured by adding 2M $HClO_4$ to halt the reaction and evolved ^{14}C-CO_2 was captured in PCR tubes with 1M NaOH and transferred to scintillation vials, as previously described (Hoehn et al., 2010). *De novo* lipogenesis from substrates was measured by hexane:isopropanol (3:2) extraction of ^{14}C-lipids for 1 hour. Solution was spun and the lipids in the top phase were transferred to scintillation vials. For measurements of glycolysis, reactions were stopped with 1N HCl, and D-[3-^{3}H] glucose was separated from tritiated [^{3}H]$_2$O (generated from dehydration at enolase in glycolytic reaction) by diffusion, as previously described (Wang et al., 2011). Samples were counted using a LS 6500 Multi-purpose Scintillation Counter (Beckman Coulter) and substrate metabolism for each sample (pmol of substrate disintegrated per minute) normalized to protein content (mg) per well.

Glucose transporter qPCR primer sequences

GLUT1 (fwd) 5′- CACCACCTCACTCCTGTTAC-3′, GLUT1 (rev) 5′-CCACTTACTTCTGTCTCACTCC-3′, GLUT4 (fwd) 5′-CTGGGCCTCACAGTGCTAC-3′, GLUT4

(rev) 5′-GTCAGGCGCTTCAGACTCTT-3′, GLUT8 (fwd) 5′-TCATGGCCTTTCTCGTGAC-3′, GLUT8 (rev) 5′-TCCTTTAGTTTCAGGGACACAG-3′.

Cytotoxicity assays

Cells (2,500-5,000/well) were seeded in 96-well plates and incubated at 37°C overnight prior to drug treatment. Drugs diluted in cell culture medium were added to each well at the indicated concentrations. Following 48-72 hours incubation at 37°C, cell viability was detected by addition of thiazoyl blue tetrazolium bromide (MTT) reagent for 3 hours. Formazan crystals were solubilized in solvent (4mM HCl, 0.1% NP-40 in isopropanol) and absorbance read at 590/620nm using a SpectraMax M5 plate reader (Molecular Devices, Sunnyvale, CA, USA). Cell viability of drug-treated cells is displayed as a percentage of control cells i.e. cells with equivalent concentrations of the appropriate drug vehicle.

Cellular ATP levels

ATP levels in lysed cells were measured using CellTiter-Glo Luminescent Cell Viability Assay reagent (Promega, Madison, WI, USA) and luminescence measured for 500ms. ATP concentrations were calculated from a standard curve.

ROS assays

Cells were seeded in 96-well plates at 5000/well a day prior to experiment. Media was removed from wells, cells were rinsed with phenol red-free DMEM (containing 25mmol/L glucose and 4mmol/L glutamine) before adding 10µmol/L CM-H2DCFDA (Life Technologies) diluted in the aforementioned media. Cells were incubated in dye for 1 hour in the dark at

37°C. Dye was removed from wells, cells were rinsed with KRP buffer (containing 25mmol/L glucose and 4mmol/L glutamine), and then incubated in BrPA (100µmol/L) diluted in the aforementioned buffer. Fluorescence (495/520nm) was monitored over the indicated time points.

Mass spectrometry of Acetyl-CoA and Pyruvylated-CoA

Analyses were performed using a triple quadrupole mass spectrometer (AB-Sciex 4000 Q-Trap) coupled to a Shimadzu LC-20AD LC system equipped with a Supelco Discovery C18 column (50 mm × 2.1 mm × 5 µm bead size). A binary solvent system (total flow 0.25 ml/min) was used that consisted of the following solvents, A: 98.6% H_2O, 2% acetonitrile, 5 mM acetic acid, 10 mM N,N-Diisopropylethylamine, 10 mM ammonium acetate; B: 75% acetonitrile, 25% solvent A. Chromatographic runs started at 100% A for 1 min, a linear gradient to reach 100 % at 3.5 min, then 100% B for 2 min, and finally 100% solvent A for 2.5 min (8 min total). Measurements were carried out in positive mode using a previously published transition for Acetyl-CoA, m/z 810.4→ m/z 303.2, (Gao et al., 2007) and the following settings (in volts): DP: 91, EP: 10; CE:43 ; CXP: 8. Quantification was carried out by measuring peak areas using the software Analyst 1.5.1 that were corrected for recovery using ^{13}C-Malonyl-CoA as Internal Standard. Retention time for Acetyl CoA was 3.3 min. Samples of 296 cells were prepared by seeding 1 × 10^6 cells per 10cm dish a day prior to drug treatment. Cells were treated with the indicated concentrations of BrPA (diluted in KRP nutrient solution) for 90 minutes, rinsed with ice-cold PBS and lysed with ice-cold 6% perchloric acid containing ^{13}C3-malonyl-CoA (0.5µM final) as an Internal Standard. Lysates were centrifuged (16,000 × g) and ultracentrifuged (100,000 × g) at 4°C and supernatants loaded onto pre-equilibrated solid-phase extraction

columns (Oasis HLB, 1cc/30mg, Waters, Milford, MA). Columns were rinsed with MQ-H_2O and eluted with acetonitrile. Eluates were dried under nitrogen gas at 37°C and reconstituted in 120 µL of chromatography solvent A and analyzed by LC/MS. The analysis of Pyruvylated-CoA was carried out by Product Ion scans as shown in Figure S6. Samples of Pyruvylated-CoA were prepared by mixing CoA and BrPA (pH 7.5) at a 10:1µmol/L ratio (BrPA:CoA) for 1 hour at room temperature. Aliquots of this reaction medium were diluted in chromatographic solvent A for analysis by Product Ion scans.

Supplemental References

Gao, L., Chiou, W., Tang, H., Cheng, X., Camp, H. S., and Burns, D. J. (2007). Simultaneous quantification of malonyl-CoA and several other short-chain acyl-CoAs in animal tissues by ion-pairing reversed-phase HPLC/MS. Journal of chromatography B, Analytical technologies in the biomedical and life sciences *853*, 303-313.

Hoehn, K. L., Turner, N., Swarbrick, M. M., Wilks, D., Preston, E., Phua, Y.*, et al.* (2010). Acute or chronic upregulation of mitochondrial fatty acid oxidation has no net effect on whole-body energy expenditure or adiposity. Cell metabolism *11*, 70-76.

Wang, R., Dillon, C. P., Shi, L. Z., Milasta, S., Carter, R., Finkelstein, D.*, et al.* (2011). The transcription factor Myc controls metabolic reprogramming upon T lymphocyte activation. Immunity *35*, 871-882.

Supplemental Figures

Byrne et al. Metabolic vulnerabilities in endometrial cancer.

Figure S1. Protein expression in human endometrial tissue. (**A**) Summary of protein expression in endometrial tumor tissue relative to normal adjacent tissue for each of the 6 patients (from Figure 1C, D and F). Protein expression was quantified for each sample using Odyssey software (LI-COR). Green indicates tumor protein expression higher than 1.5-fold compared to matched non-tumor tissue, while red indicates tumor protein expression lower than 0.5-fold compared with matched non-tumor tissue. *indicates the phosphorylation of proteins relative to total protein expression. GT= glucose transporter. (**B**) The expression of other metabolic regulatory proteins in tumor (*T*) and normal adjacent (*N*) endometrial tissue (6 patients total). 14-3-3 serves as a protein loading control.

Figure S1.

A

	GLYCOLYSIS				GT	
Protein	**HK2**	**GAPDH**	**PKM2**	**LDHA**	**GLUT6**	**GLUT1**
Patient 1	2.2	0.7	2.1	1.5	3.0	0.9
Patient 2	9.8	1.3	3.5	4.6	3.5	4.0
Patient 3	2.0	0.8	1.4	0.5	0.8	0.7
Patient 4	1.4	0.6	0.9	2.6	2.5	1.0
Patient 5	12.4	2.0	5.1	17.3	4.6	4.6
Patient 6	7.5	3.4	8.5	13.0	12.9	2.6

	DE NOVO LIPOGENESIS			
Protein	**ACLY**	**ACC1**	**ACC2**	**FASN**
Patient 1	1.5	1.8	3.3	1.5
Patient 2	2.7	1.8	1.7	3.5
Patient 3	0.8	1.0	1.1	0.7
Patient 4	1.4	1.3	1.5	2.0
Patient 5	2.1	2.4	3.0	3.8
Patient 6	3.6	1.7	3.2	2.7

	Akt PATHWAY		
Protein	**PTEN**	**AKT**	**pAKT***
Patient 1	1.2	1.1	3.2
Patient 2	0.9	1.0	5.8
Patient 3	0.9	0.9	0.9
Patient 4	1.5	1.1	1.1
Patient 5	1.1	0.6	16.0
Patient 6	0.5	1.3	3.8

B

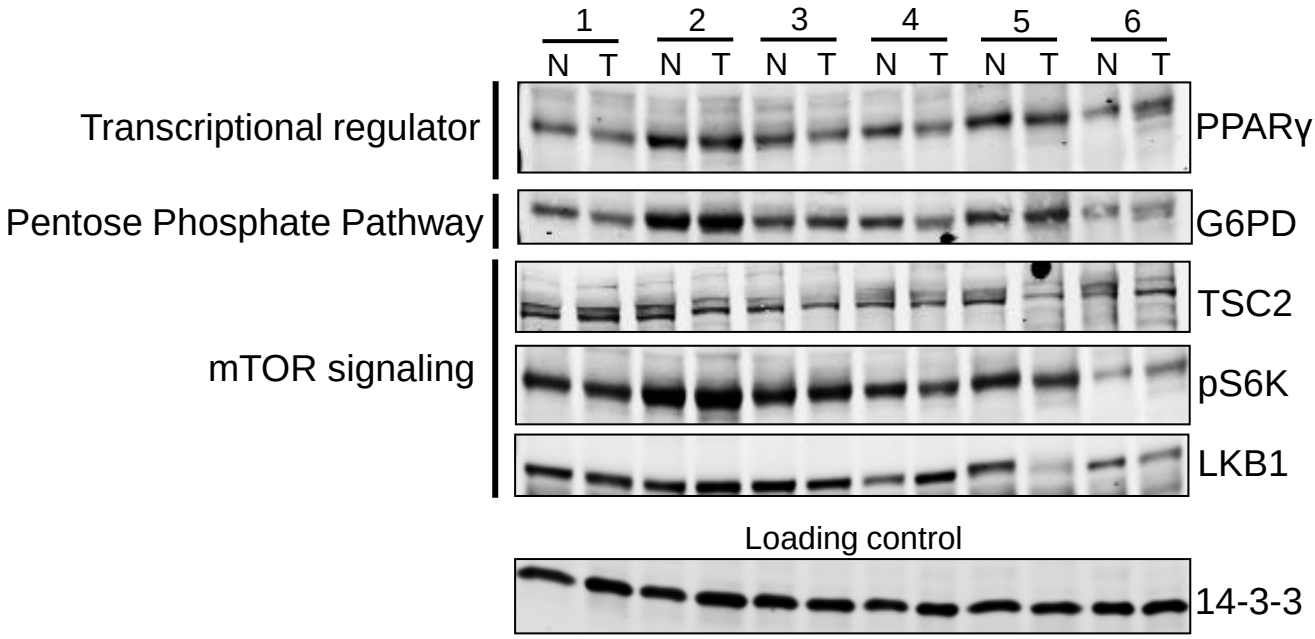

Figure S2. GLUT6 expression in human endometrial tissue. Matched tumor and non-tumor endometrium from 2 obese postmenopausal women. GLUT6 staining is strong in blood vessels (*arrow heads*) of the non-tumor endometrium (*left panel*). Strong GLUT6 staining is evident in cancerous glandular epithelial cells (*E*), blood vessels (*arrow heads*), and weaker staining is seen in stromal cells (*S*) in the Type I (endometrioid) tumors.

Figure S2.

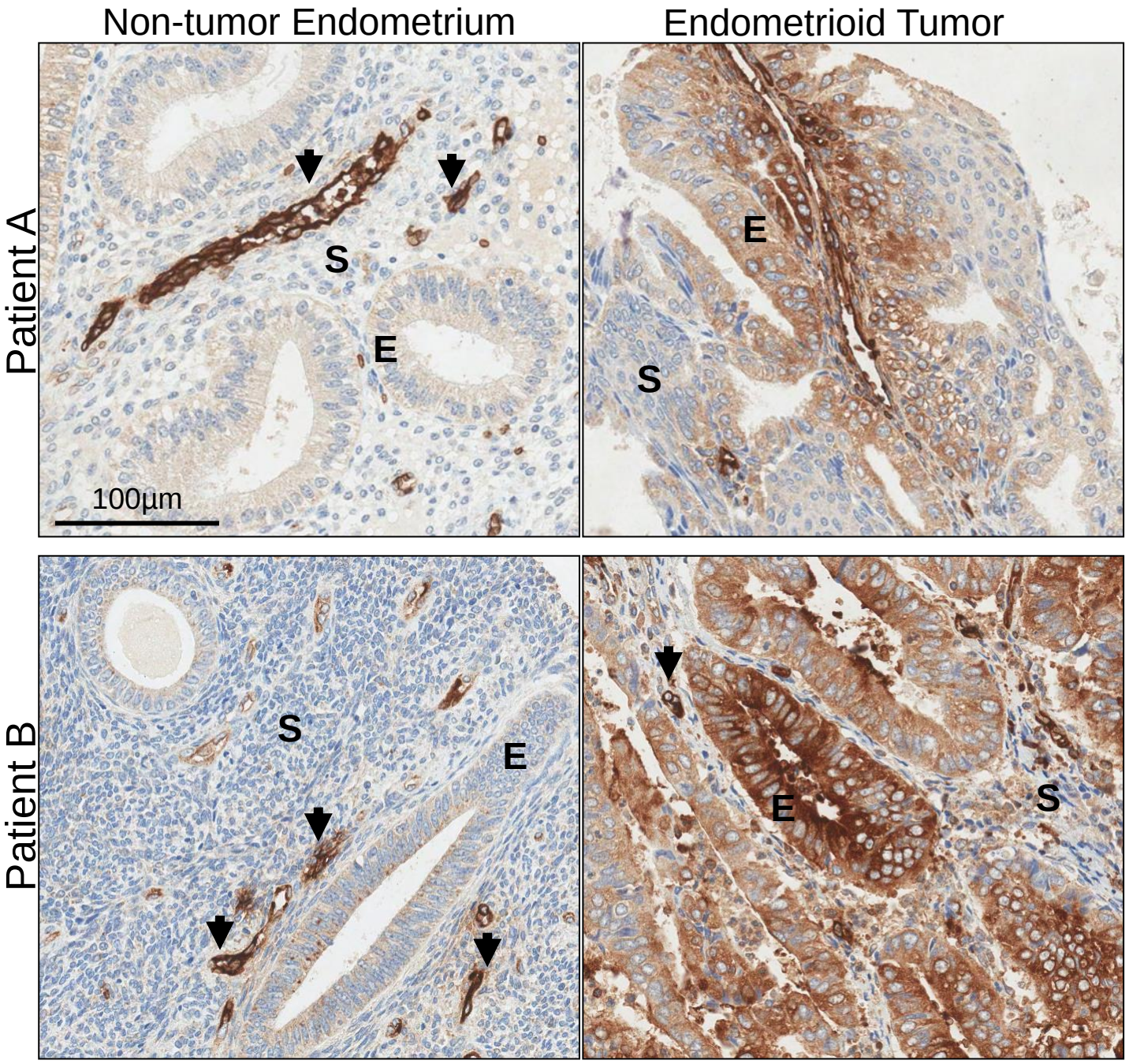
Non-tumor Endometrium
Endometrioid Tumor
Patient A
Patient B
S
E
100µm

Figure S3. Correlation between metabolic protein expression and metabolism in endometrial cells. Protein expression (average of 3 independent immunoblots) was evaluated in human endometrial cancer (*HEC, ISH, 296, 319, AN3, KLE, RL*) and non-cancerous epithelial (*hUE*) and stromal (*MAD*) cells and was analyzed for correlations with glucose metabolism; glucose oxidation (pmol ^{14}C-glucose to $^{14}CO_2$/min/mg protein), glycolysis (pmol 3-^{3}H-glucose to ^{3}HOH/min/mg protein), or glucose metabolism to lipid (pmol ^{14}C-glucose to ^{14}C-lipid/min/mg protein). Metabolic assays represent the mean (±SEM) of 3 technical replicates (experiments were performed at least twice). Pearson correlation coefficients (r values) and significance (p values) were calculated using GraphPad Prism software. GLUT6 protein expression correlated with Warburg metabolism [low glucose oxidation (glucose->CO_2)/high glycolysis (glucose->H_2O) ratio] (**A**). The phosphorylation of Akt (pAkt/Akt) correlated with glycolysis (**B**) and glucose conversion to lipids (**C**).

Figure S3.

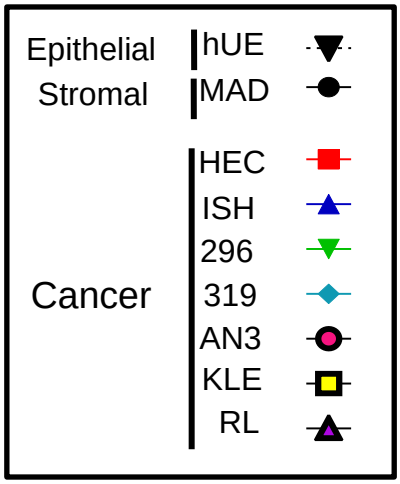
Epithelial
Stromal
Cancer
hUE
MAD
HEC
ISH
296
319
AN3
KLE
RL

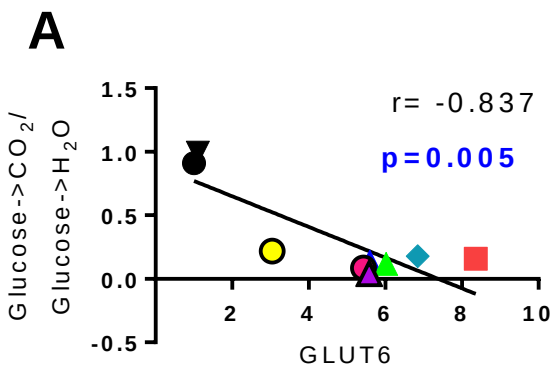
A
r= -0.837
p=0.005
Glucose->CO2/
Glucose->H2O
GLUT6

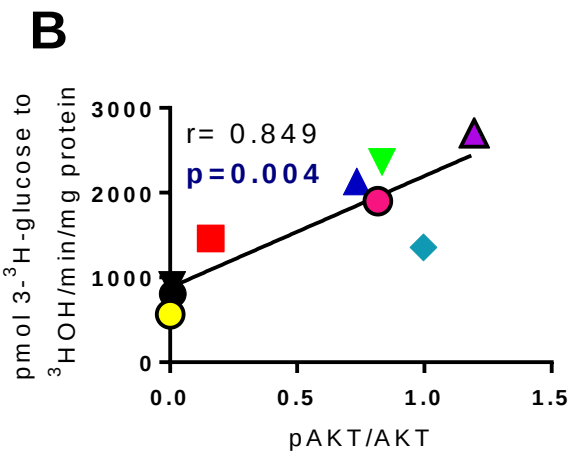
B
r= 0.849
p=0.004
pmol 3-3H-glucose to
3HOH/min/mg protein
pAKT/AKT

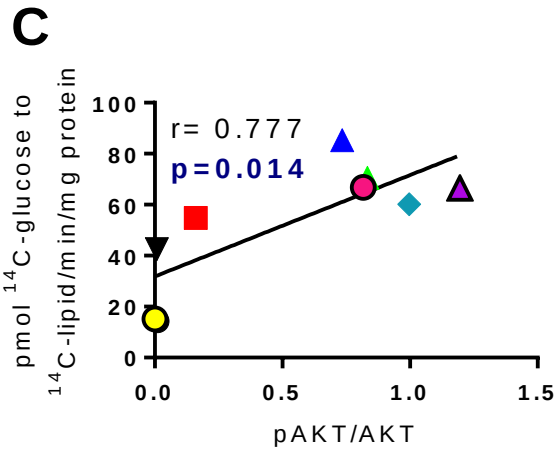
C
r= 0.777
p=0.014
pmol 14C-glucose to
14C-lipid/min/mg protein
pAKT/AKT

Figure S4. GLUT6 knockdown in endometrial cancer cells induces cell death. (**A**) 296 cells were transfected with control siRNA (Ctrl), a pool of 4 GLUT6 siRNA sequences (Pool), or each of the 4 individual GLUT6 siRNA sequences separately. Maximum GLUT6 protein knockdown was observed using Sequence 4 siRNA (Seq.4), 96 hr post-transfection. β-actin served as a protein loading control. (**B**) GLUT1, GLUT4 and GLUT8 mRNA expression were not significantly altered in 296 cells transfected with GLUT6 Pool siRNA, compared with controls. (**C**) Representative micrographs showing 296 cell death (dynamic membrane blebbing) following GLUT6 knockdown with Seq.4 siRNA. (**D**) RL cells were transfected with siRNA as described in (A). (**E**) GLUT6 knockdown reduced viable RL cell counts by 59% (Pool siRNA) and 83% (Seq.4 siRNA) at 96 hr post-siRNA transfection, compared with controls. (**F**) GLUT6 knockdown increased sub-G1 cell populations, as determined by cell cycle analysis (80 hr post-transfection). Sub-G1 populations are indicated (*red bar*) and population counts are shown within the histogram. (**G**) GLUT6 knockdown increased the number of Annexin V positive (AV+) cells (80 hr post-transfection). Data are presented as percentage of total cells (AV+ plus AV-). (**H**) LDH release in GLUT6 siRNA-transfected RL cells was calculated as a fold-increase of controls, 96 hr post-transfection. All data represent the mean of at least three independent experiments ± SEM (*$p<0.05$). *NS*= not significant.

Figure S4.

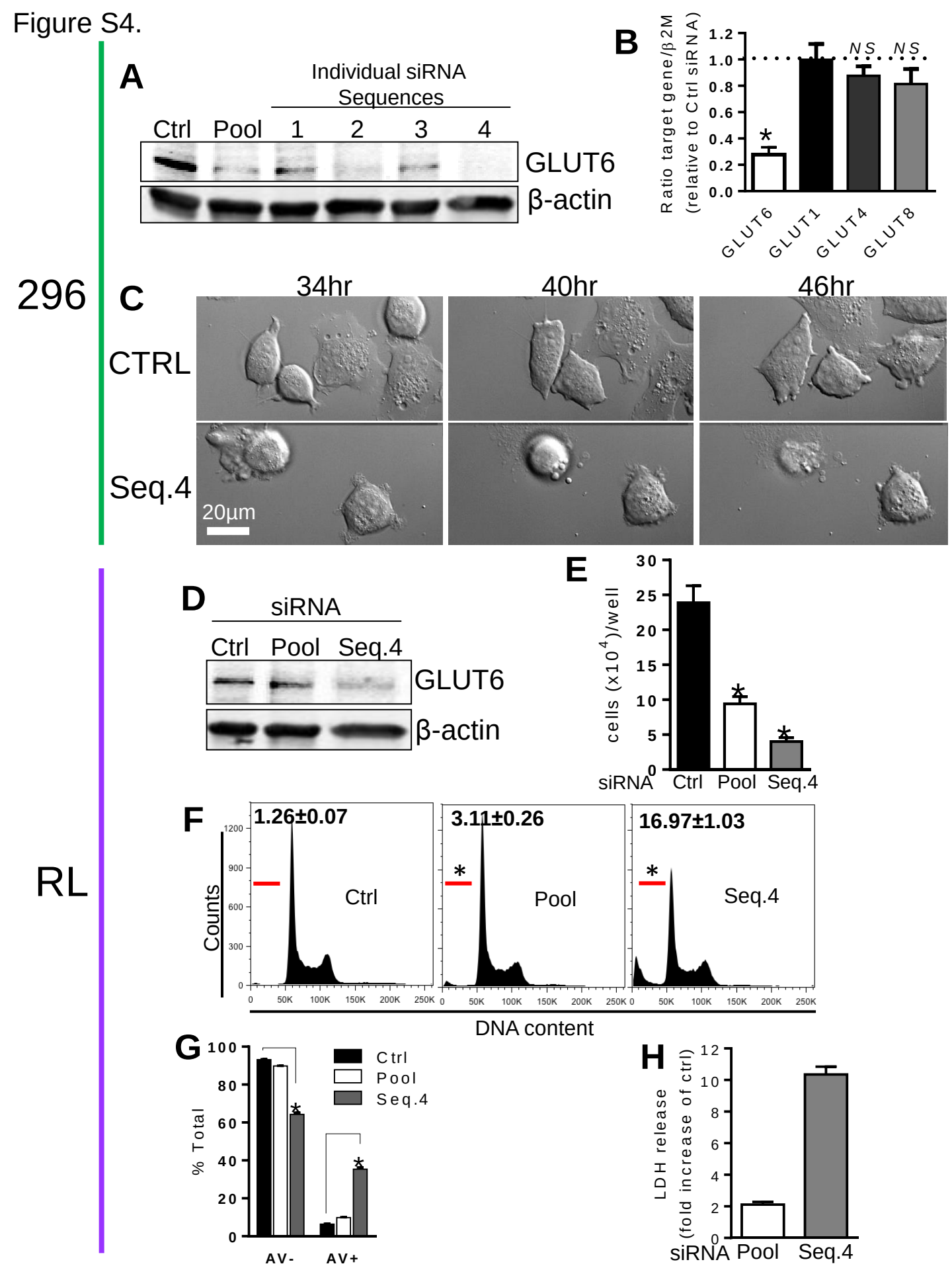
A
Individual siRNA Sequences
Ctrl
Pool
1
2
3
4
GLUT6
β-actin
B
Ratio target gene/β2M (relative to Ctrl siRNA)
1.2
1.0
0.8
0.6
0.4
0.2
0.0
*
NS
NS
GLUT6
GLUT1
GLUT4
GLUT8
296
C
34hr
40hr
46hr
CTRL
Seq.4
20µm
RL
D
siRNA
Ctrl
Pool
Seq.4
GLUT6
β-actin
E
cells (x10^4)/well
30
25
20
15
10
5
0
*
*
siRNA
Ctrl
Pool
Seq.4
F
1.26±0.07
3.11±0.26
16.97±1.03
Ctrl
Pool
Seq.4
Counts
1200
900
600
300
0
50K
100K
150K
200K
250K
DNA content
G
% Total
100
80
60
40
20
0
Ctrl
Pool
Seq.4
*
*
AV-
AV+
H
LDH release (fold increase of ctrl)
12
10
8
6
4
2
0
siRNA
Pool
Seq.4

Figure S5. Correlation analyses for drug sensitivity. (**A**) Population doubling time of human endometrial cells (hours). Data represent the mean of 3 biological replicates (±SEM). (**B**) Population doubling time of endometrial cells significantly correlates with their sensitivity to paclitaxel (IC_{50} nmol/L). (**C**) MCT1 protein expression in human endometrial cell lines. 14-3-3 serves as a loading control. (**D**) Endometrial cell sensitivity to BrPA [(*BrPA* IC_{50} *(μM)*] did not significantly correlate with MCT1, HK2 and GAPDH protein expression. Representative western blots for these analyses are shown in Figures 2A and S5C. Arbitrary protein expression scores were given to each cell line (mean value from 3 independent lysates and blots), with the highest expressing cell line for each protein given a score of 1 (*red color shading*). The lowest protein expression is represented by blue color shading. Pearson correlation coefficients (r values) and significance (p values) were calculated using GraphPad Prism software.

Figure S5.

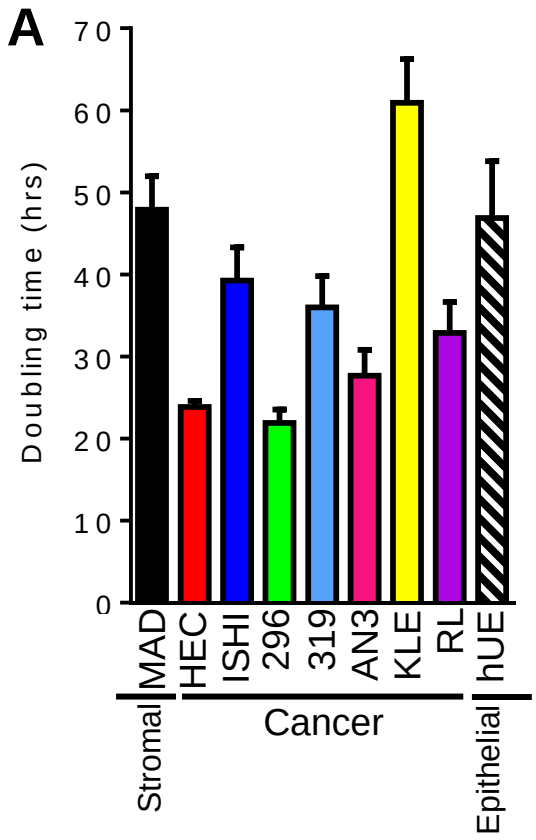

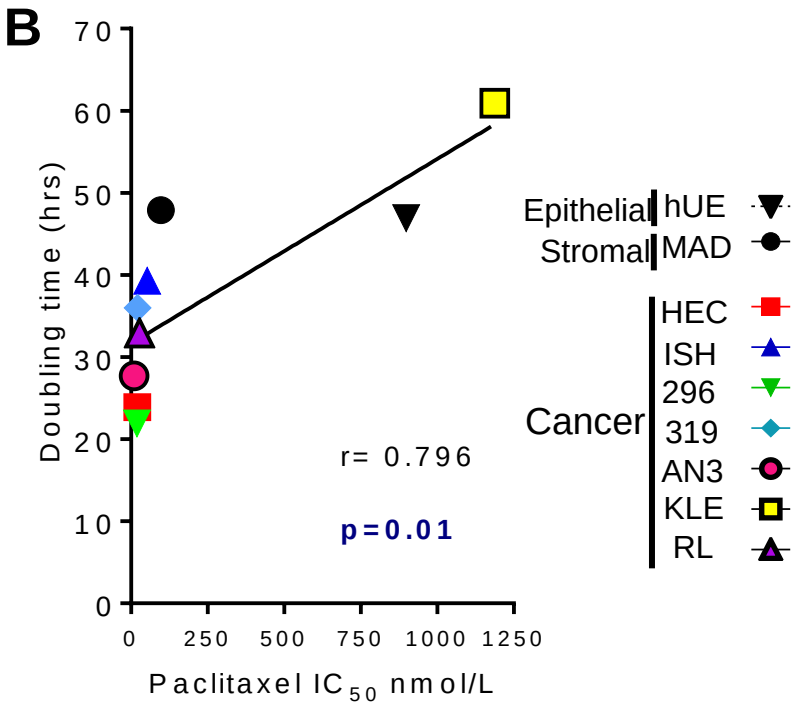

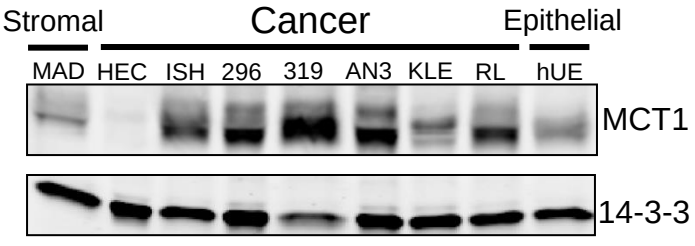

D

Cell Line	BrPA IC_{50} (μM)	Arbitrary Protein Expression		
		MCT1	HK2	GAPDH
KLE	34	0.62	0.52	0.72
296	42	0.88	0.84	1.00
AN3	72	0.97	1.00	0.88
RL95	99	0.83	0.80	0.25
hUE	106	0.62	0.51	0.12
MAD	221	0.58	0.67	0.31
ISHI	230	0.74	0.69	0.21
319	268	1.00	0.66	0.55
HEC	1267	0.37	0.36	0.35
p value		0.06	0.08	0.40
r value		-0.64	-0.61	-0.32

Figure S6. Precursor Ion Scan of Pyruvylated-CoA. A sample of the solution in which CoA and BrPA were allowed to react, was analyzed by a Product Ion Scan. Low collision energy was used to observe both the parent and the product ions. Observed peaks correspond to the calculated masses that can be predicted using published data for CoA (Burns et al., 2005). The parent and the sulfur-containing ions of CoA were increased by 86 m/z units upon reaction with BrPA, whereas the m/z 428 ion remained unchanged indicating that the pyruvylation reaction occurred at the sulfur atom.

Figure S6.

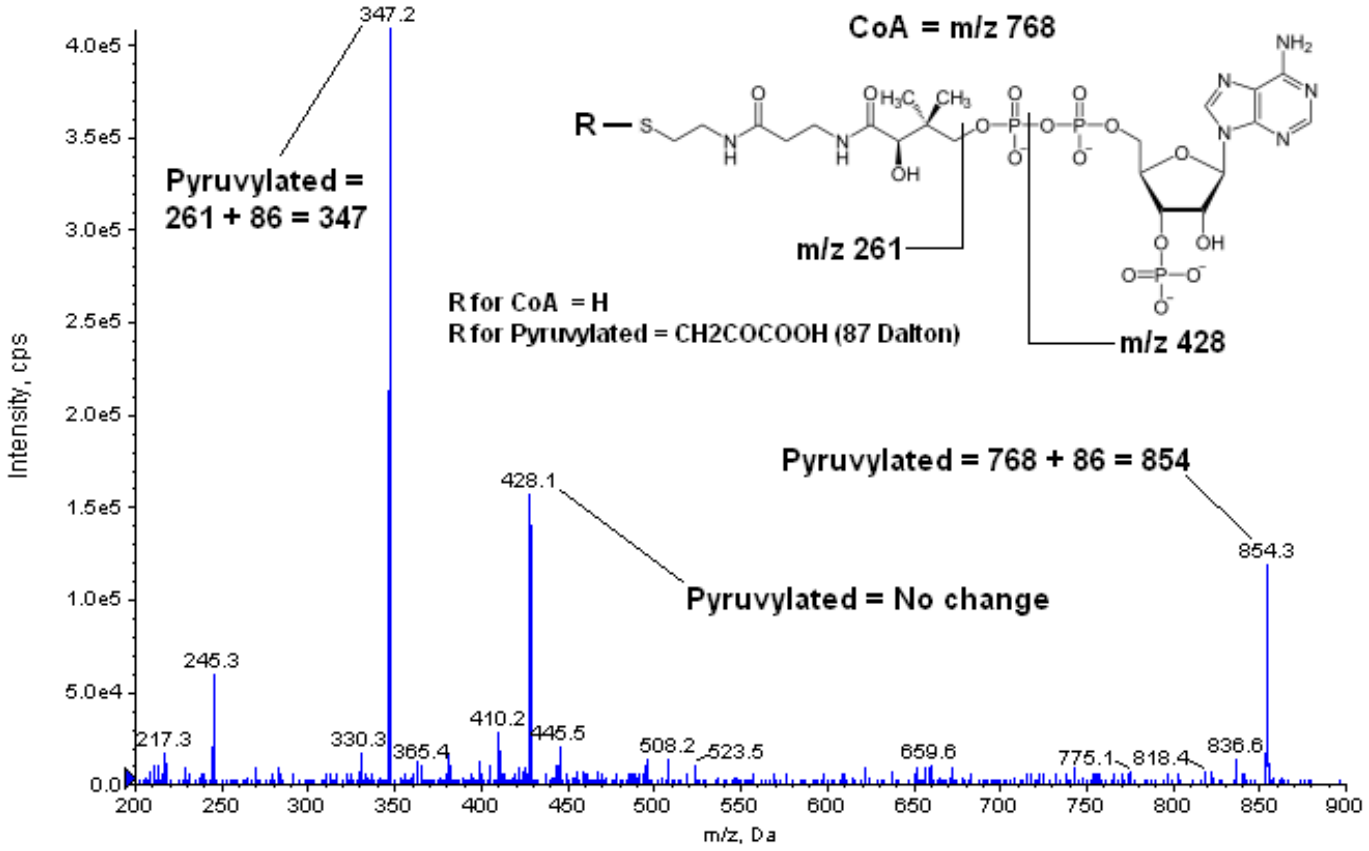
CoA = m/z 768
Pyruvylated =
261 + 86 = 347
m/z 261
m/z 428
R for CoA = H
R for Pyruvylated = CH2COCOOH (87 Dalton)
Pyruvylated = 768 + 86 = 854
Pyruvylated = No change
Intensity, cps
m/z, Da
347.2
428.1
854.3
245.3
217.3
330.3
365.4
410.2
445.5
508.2
523.5
659.6
775.1
818.4
836.6

Figure S7. Antioxidants (without thiol groups) could not protect against 3-bromopyruvate-mediated cell death. (**A**) CMH2DCFDA-loaded 296 cells were treated with BrPA (100μM) and the change in fluorescent signal was measured at the indicated time points (% increase of untreated cells). (**B**) Representative micrographs (phase contrast and GFP filter) of 296 cells loaded with CMH2DCFDA and left untreated or treated with BrPA (100μM). (**C-I**) 296 cells were pretreated with apopcynin (300μM), allopurinol (1mM), L-NAME (100μM), MnTBAP (100μM), Mito-tempo (100μM), resveratrol (20μM) and L-ascorbic acid (100μM) for 30 minutes prior to treatment with increasing doses of BrPA. Cell viability (MTT assay) was determined 48 hours later.

Figure S7.

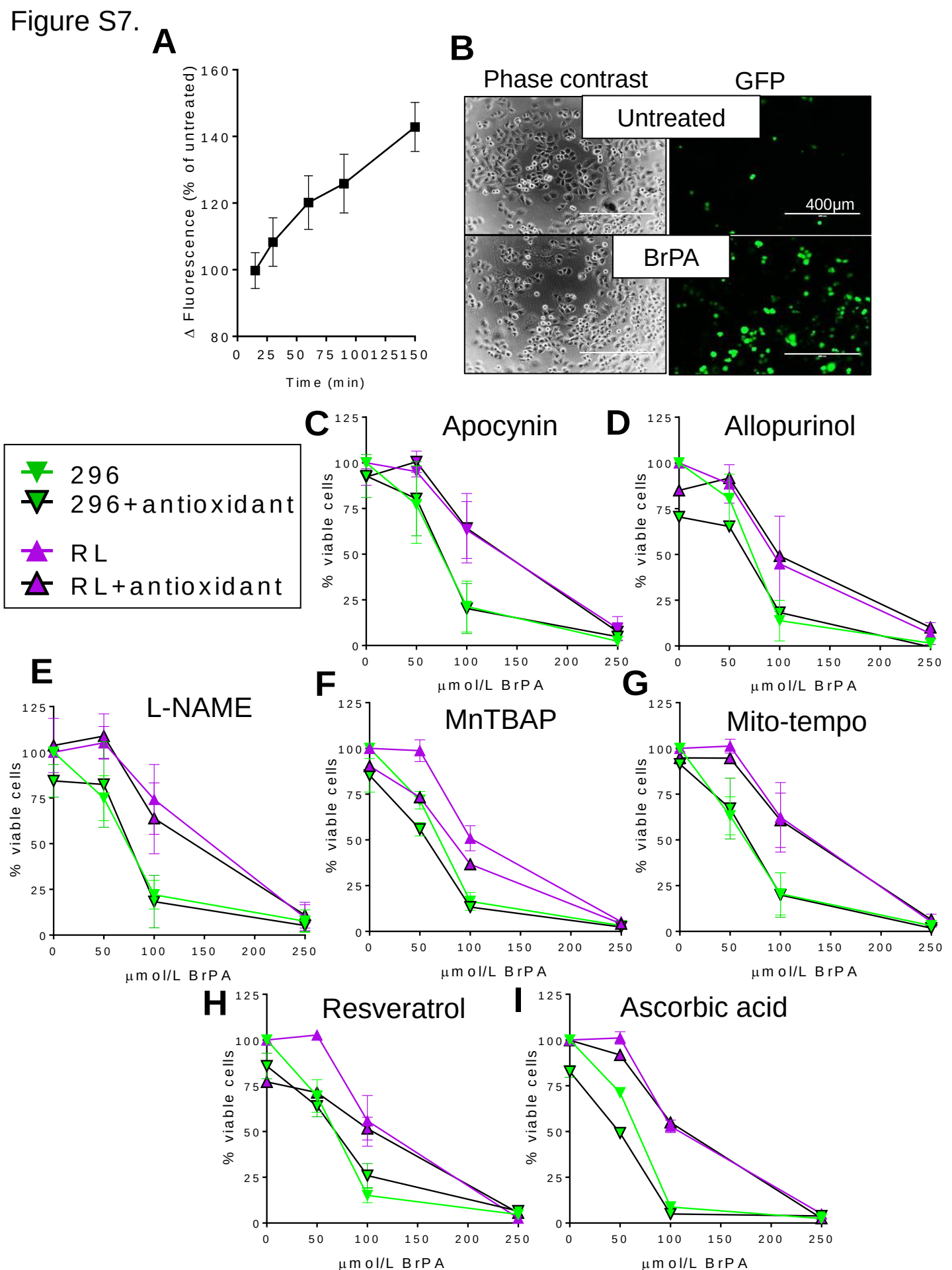
A
Δ Fluorescence (% of untreated)
160
140
120
100
80
0 25 50 75 100 125 150
Time (min)
B
Phase contrast
GFP
Untreated
400µm
BrPA
296
296+antioxidant
RL
RL+antioxidant
C
Apocynin
D
Allopurinol
E
L-NAME
F
MnTBAP
G
Mito-tempo
H
Resveratrol
I
Ascorbic acid
% viable cells
µmol/L BrPA

Figure S8. ATP levels and cell death induced by 3-bromopyruvate. (**A**) ATP levels in 296 cells untreated or treated with 100 μM BrPA for the indicated times. (**B**) Representative micrographs of UV-irradiated 296 cells with or without Q-VD-OPH (QVD) at time zero (0 hr) and 6 hrs. (**C**) LDH release at 18hrs in RL cells treated with 250μM 3-bromopyruvate (BrPA) (+/-QVD) or UV-irradiated (+/-QVD). LDH release is calculated as a % increase of untreated cells. Data represent the mean of at least three independent experiments (error bars ± SEM) (*$p<0.05$). NS= not significant.

Figure S8.

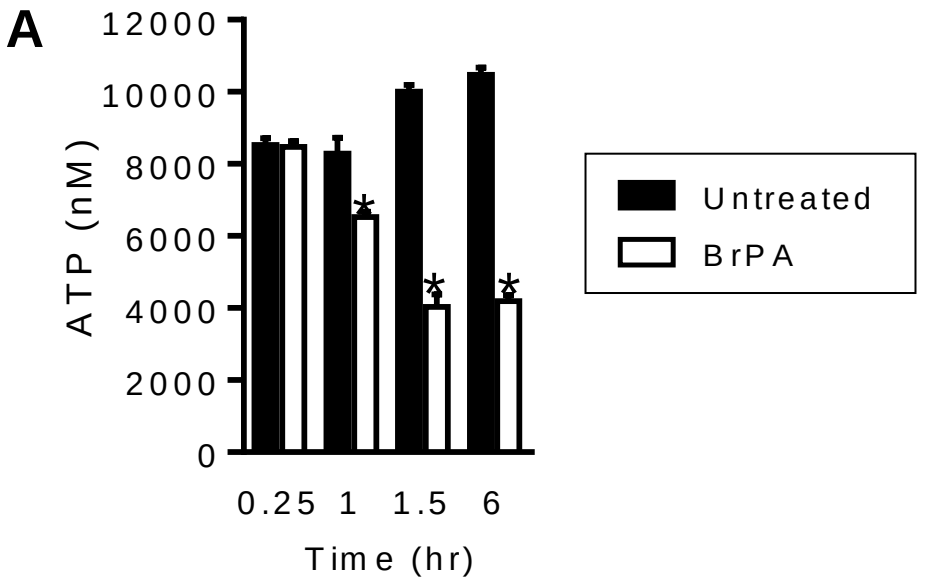
A
12000
10000
8000
6000
4000
2000
0
ATP (nM)
0.25
1
1.5
6
Time (hr)
Untreated
BrPA

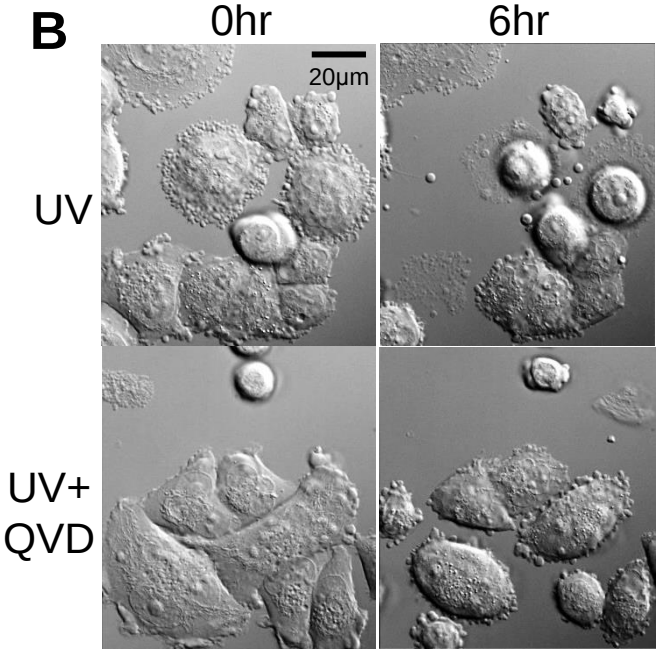
B
0hr
6hr
20µm
UV
UV+
QVD

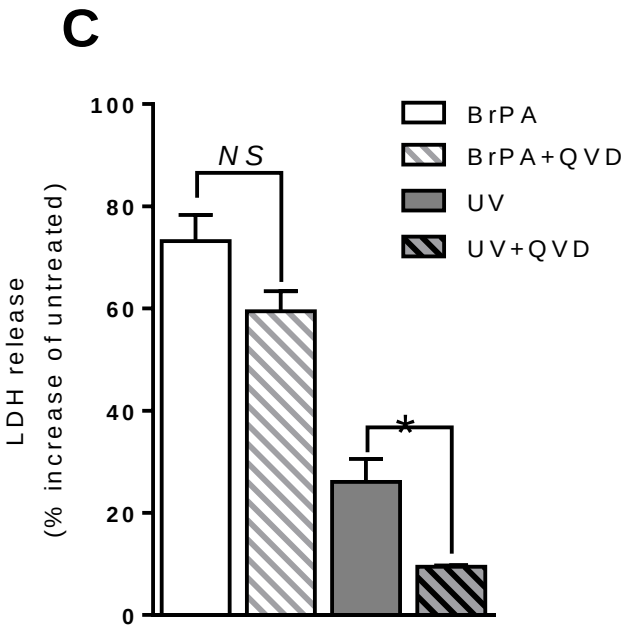
C
100
80
60
40
20
0
LDH release
(% increase of untreated)
NS
*
BrPA
BrPA+QVD
UV
UV+QVD